

~~CONFIDENTIAL~~~~CONFIDENTIAL~~  
NACA

## RESEARCH MEMORANDUM

STATIC LATERAL STABILITY AND CONTROL CHARACTERISTICS OF  
A MODEL OF A 45° SWEEP-WING FIGHTER AIRPLANE  
WITH VARIOUS VERTICAL TAILS AT MACH NUMBERS  
OF 1.41, 1.61, AND 2.01

By M. Leroy Spearman and Ross B. Robinson

Langley Aeronautical Laboratory  
Langley Field, Va.

UNCLASSIFIED

To

by authority of *Naval Air Command*  
*U.S. 9-11 59*

CLASSIFIED DOCUMENT

This material contains information affecting the National Defense of the United States within the meaning of the espionage laws, Title 18, U.S.C., Secs. 793 and 794, the transmission or revelation of which in any manner to an unauthorized person is prohibited by law.

NATIONAL ADVISORY COMMITTEE  
FOR AERONAUTICS

WASHINGTON

June 19, 1956

~~CONFIDENTIAL~~



3 1176 01437 2172

## NATIONAL ADVISORY COMMITTEE FOR AERONAUTICS

## RESEARCH MEMORANDUM

STATIC LATERAL STABILITY AND CONTROL CHARACTERISTICS OF  
A MODEL OF A  $45^\circ$  SWEEP-WING FIGHTER AIRPLANE  
WITH VARIOUS VERTICAL TAILS AT MACH NUMBERS  
OF 1.41, 1.61, AND 2.01

By M. Leroy Spearman and Ross B. Robinson

## SUMMARY

An investigation has been made in the Langley 4- by 4-foot supersonic pressure tunnel at Mach numbers of 1.41, 1.61, and 2.01 of a model of a  $45^\circ$  swept-wing fighter airplane. The wing had an aspect ratio of 3.86, a taper ratio of 0.262, and NACA 64(06)A007 airfoil sections in a streamwise direction. Static lateral stability and control characteristics were obtained through an angle-of-attack and sideslip range for various combinations of component parts and for the complete model with three different vertical tails of varying sizes and aspect ratios. The majority of the tests were conducted at a Mach number of 1.61, and only limited sideslip results were obtained at Mach numbers of 1.41 and 2.01. Aileron- and rudder-control characteristics were obtained for the complete model at a Mach number of 1.61 only.

The directional stability derivative  $C_{n\beta}$  for the complete configuration progressively decreased with increasing Mach number and angle of attack until regions of directional instability occurred. Increasing the size of the vertical tail provided increases in  $C_{n\beta}$  so that the onset of directional instability was delayed to higher Mach numbers or angles of attack.

The lateral and directional control characteristics were essentially constant throughout the angle-of-attack and sideslip ranges.

~~CONFIDENTIAL~~

## INTRODUCTION

A research program has been undertaken in the Langley 4- by 4-foot supersonic pressure tunnel to determine the aerodynamic characteristics of a model of a  $45^\circ$  swept-wing fighter airplane in the Mach number range from 1.41 to 2.01. The static longitudinal stability and control characteristics at Mach numbers of 1.41, 1.61, and 2.01 are presented in reference 1. Effects of various external stores on the longitudinal and lateral characteristics at Mach numbers of 1.61 and 2.01 have been determined but the results are unpublished. Flight-test results of a similar configuration are presented in reference 2.

The present paper contains the static lateral and directional stability and control characteristics at Mach numbers of 1.41, 1.61 and 2.01. The Reynolds numbers of the tests based on the wing mean geometric chord varied from  $1.40 \times 10^6$  to  $1.16 \times 10^6$ . Results were obtained for the model equipped with three different vertical tails of varying area and aspect ratio.

## COEFFICIENTS AND SYMBOLS

The lift, drag, and pitching-moment coefficients are referred to the stability axis system (fig. 1(a)). The lateral-force, yawing-moment, and rolling-moment coefficients are referred to the body axis system except where noted (fig. 1(b)). The center of moments of the model was at a longitudinal position corresponding to the 37.5-percent station of the wing mean geometric chord. The coefficients and symbols are defined as follows:

$C_L$  lift coefficient,  $-F_Z/qS$

$C_X$  longitudinal-force coefficient,  $F_X/qS$

$C_m$  pitching-moment coefficient,  $\frac{M_Y}{qS\bar{c}}$

$C_n$  yawing-moment coefficient,  $\frac{M_Z}{qSb}$

$C_l$  rolling-moment coefficient,  $\frac{M_X}{qSb}$

$C_Y$	lateral-force coefficient, $\frac{F_Y}{qS}$
$F_Z$	force along Z-axis
$F_X$	force along X-axis ( $-F_X$ = Drag at $\beta = 0^\circ$ )
$M_Y$	pitching moment about Y-axis
$M_Z$	yawing moment about Z-axis
$M_X$	rolling moment about X-axis
$F_Y$	force along Y-axis
$q$	dynamic pressure
$S$	wing area, sq ft
$\bar{c}$	wing mean geometric chord
$b$	wing span
$M$	Mach number
$\alpha$	angle of attack of wing chord plane, deg
$\beta$	angle of sideslip, deg
$i_t$	horizontal-tail incidence angle with respect to fuselage reference line, deg
$\delta_{aL}$	left aileron deflection, normal to hinge line, deg
$\delta_r$	rudder deflection, deg
$C_{n\beta}$	directional stability parameter, $\frac{\partial C_n}{\partial \beta}$
$C_{l\beta}$	effective dihedral parameter, $\frac{\partial C_l}{\partial \beta}$
$C_{Y\beta}$	variation of $C_Y$ with $\beta$ near $\beta = 0^\circ$ , $\frac{\partial C_Y}{\partial \beta}$
$H$	horizontal tail

V vertical tail

W wing

B body

Subscripts:

O, -10 values of  $i_t$  used with H, deg

S stability axis

W wing

V vertical tail

t horizontal tail

#### MODEL AND APPARATUS

A three-view drawing of the model is shown in figure 2. Details of the various vertical tails tested are given in figure 3. The geometric characteristics of the model are given in table I.

The wing had  $45^\circ$  of sweepback of the quarter-chord line, an aspect ratio of 3.86, a taper ratio of 0.262, NACA 64(06)A007 airfoil sections in a streamwise direction, and had zero twist, incidence, and dihedral. The wing chord plane was approximately 0.10 wing semispans below the fuselage reference line. The ailerons were of the trailing-edge flap type and could be manually deflected on the model.

Both the horizontal and vertical tails had  $45^\circ$  of sweepback of the quarter-chord line and NACA 65A003.5 airfoil sections in a streamwise direction. The all-movable horizontal tail was located 0.0258 wing semispans below the wing chord plane extended and was manually adjustable.

Three vertical-tail configurations were investigated: (1) a basic tail, (2) an extended tip modification, and (3) a 127-percent modification which had an area about 27 percent greater than that of the basic vertical tail. (See fig. 3 and table I.) The rudder could be manually deflected.

Forces and moments were measured by a six-component strain-gage balance contained in the sting-supported model. For the tests at

$M = 1.61$  and  $2.01$ , the model was mounted on a remotely controlled rotary sting; whereas for the tests at  $M = 1.41$ , a manually adjustable sting was employed.

### TESTS, CORRECTIONS, AND ACCURACY

The conditions for the tests were as follows:

Mach number . . . . .	1.41	1.61	2.01
Stagnation temperature, $^{\circ}\text{F}$ . . . .	100	100	100
Stagnation pressure, lb/sq in.			
abs . . . . .	6	6	6
Stagnation dewpoint, $^{\circ}\text{F}$ . . . . .	-20	-20	-25
Reynolds number, based on $\bar{c}$ . . . .	$1.40 \times 10^6$	$1.34 \times 10^6$	$1.16 \times 10^6$

Tests were made through the following approximate angle ranges:

M	Variable angle range, deg	Constant angle, deg
1.41	$\beta \approx -8$ to $15$ $\alpha \approx -8$ to $16$	$\alpha \approx 5.1$ $\beta \approx -4.8, 0$
1.61	$\beta \approx -20$ to $20$ $\beta \approx 0$ to $15$ $\beta \approx 0$ to $12$	$\alpha \approx 0$ $\alpha \approx 4.1, 8.3, 15.7$ $\alpha \approx 20.9$
2.01	$\beta \approx 0$ to $20$ $\beta \approx 0$ to $15$	$\alpha \approx 0$ $\alpha \approx 4.1, 8.2$

The model angle was corrected for the deflection of the balance and sting under load. Base pressure was measured in the plane of the model base. By equating the base pressure to free-stream static pressure, the drag values have been adjusted so that the base drag was zero for all configurations.

Maximum probable errors in the individual measured quantities are as follows:

	M = 1.41 and 1.61	M = 2.01
$C_L$ . . . . .	$\pm 0.0044$	$\pm 0.0051$
$C_X$ . . . . .	$\pm 0.0005$	$\pm 0.0007$
$C_m$ . . . . .	$\pm 0.0017$	$\pm 0.0021$
$C_n$ . . . . .	$\pm 0.0003$	$\pm 0.0003$
$C_l$ . . . . .	$\pm 0.0002$	$\pm 0.0002$
$C_Y$ . . . . .	$\pm 0.0020$	$\pm 0.0020$
$\alpha, \beta, \text{ deg}$ . . . . .	$\pm 0.2$	$\pm 0.2$
$i_t, \delta a_L, \text{ deg}$ . . . . .	$\pm 0.1$	$\pm 0.1$
M . . . . .	$\pm 0.01$	$\pm 0.015$

## RESULTS AND DISCUSSION

As seen in table II, the basic data are presented in figures 4 to 11; the summary data, in figures 12 to 18; the aileron-control data, in figures 19 to 21; and the rudder-control data, in figures 22 to 24.

### Static Stability Characteristics

Directional stability.- The directional stability  $C_{n\beta}$  for the basic configuration decreases progressively both with increasing angle of attack and increasing Mach number until regions of undesirably low stability are encountered (see fig. 15). The directional characteristics for the tail-off configuration (fig. 16) are essentially invariant with Mach number and angle of attack and indicate a relatively large unstable moment. This large unstable moment results primarily from the large fuselage and the far-rearward moment center. The far-rearward moment center also results in a short tail moment arm and, hence, lessens the ability of the vertical tail to provide a stabilizing moment. Consequently, the condition exists where a large percentage of the tail contribution is consumed in overcoming the instability of the wing-body combination and relatively little tail effectiveness is available to provide a stability margin. Under such conditions, factors that affect the tail contribution, even to a slight degree, begin to assume greater importance. For example, the rapid decrease in  $C_{n\beta}$  with increasing Mach number for the complete configuration is a direct result of the decrease to be expected in the vertical-tail lift-curve slope. In addition, as pointed out in refer-

ence 2, the losses in tail contribution resulting from aeroelasticity might be significant for a full-scale airplane.

Increasing the tail contribution through increases in the tail area and aspect ratio, although having little effect on the variations of  $C_{n\beta}$  with Mach number or angle of attack, does increase the magnitude of  $C_{n\beta}$  in such a way that the imminence of directional instability is delayed to higher angles of attack or to high Mach numbers. (See figs. 12, 13, and 17.)

The variation of  $C_n$  with  $\beta$  for the complete model is rather nonlinear and does, in fact, indicate a reversal in direction which results in the occurrence of unstable yawing moments (fig. 7, for example). This trend is influenced to some extent by the increasing instability of the wing-body combination and by a nonlinear vertical-tail contribution, and occurs even though the tail contribution continues to increase with increasing sideslip. Increasing the tail size does not remove this nonlinear variation of  $C_n$  with  $\beta$  but does delay the occurrence of the unstable yawing moments to higher angles of sideslip.

The presence of the horizontal tail provides a slight increase in the directional stability at  $\alpha = 0^\circ$  either with or without the vertical tail (figs. 6 and 10), but at higher angles of attack this effect reverses. Negative deflections of the horizontal tail provided an increase in the directional stability for the basic configuration at  $M = 1.61$  (fig. 9), apparently because of a transmittal of positive pressures from the upper surface of the horizontal tail to the windward side of the body and vertical tail. The effect of tail deflection is evident at  $M = 2.01$  (fig. 10) but to a lesser degree since a smaller portion of the body and vertical tail are influenced by the flow field of the horizontal tail as the Mach number increases.

Results from other investigations involving configurations having high horizontal tails (ref. 3, for example) indicate an opposite effect in that negative deflections of the horizontal tail cause a decrease in the directional stability.

An interesting feature concerning the effects of the axis system on the interpretation of the data is illustrated in figure 18 where the variation of  $C_{n\beta}$  with  $\alpha$  for the basic configuration at  $M = 1.61$  is presented for both the stability and the body axis systems. The results computed for the stability axis system indicate less deterioration of directional stability with increasing angle of attack and, in fact, do not indicate any directional instability for the tail-on case, whereas the results computed for the body axis system indicate directional instability above  $\alpha = 16^\circ$ . This effect results from the transfer of rolling



moment into yawing moment for the stability axis system and can cause an appreciable difference in  $C_{n\beta}$  at the higher angles of attack if the rolling moments are large and the yawing moments are small. Thus, it is possible that some configuration changes that have a large effect on roll but little effect on yaw (such as wing dihedral) may, if computed for a stability axis system, show an effect on yaw.

Effective dihedral.- The variation of  $C_{l\beta}$  with  $\alpha$  for the basic configuration is particularly nonlinear at Mach numbers of 1.41 and 1.61 (fig. 15): it varies from small negative values to small positive values at low angles of attack and increases to relatively large negative values at higher angles of attack. The results at  $M = 2.01$  are for only a limited angle-of-attack range up to about  $8^\circ$ , but within this range the variation of  $C_{l\beta}$  with  $\alpha$  is fairly linear.

For Mach numbers of 1.41 and 1.61, the variation of  $C_{l\beta}$  with  $\alpha$  at low angles of attack is generally positive either with or without the vertical tail (figs. 15 and 16); whereas for  $M = 2.01$ , the variation is negative. This trend toward negative variations of  $C_{l\beta}$  with  $\alpha$  for increasing Mach number is in general agreement with the linear-theory prediction for swept wings having supersonic leading edges (ref. 4).

The presence of the vertical tail, of course, provides a negative increment of  $C_{l\beta}$  that progressively increases as the tail size increases and progressively decreases as the Mach number increases (fig. 17).

Effects of sideslip on longitudinal characteristics.- The lift, longitudinal force, and pitching moment vary only slightly with angle of sideslip for angles of attack up to about  $8^\circ$  (figs. 4, 8, and 11). At  $\alpha = 15.7^\circ$  and  $20.9^\circ$  (fig. 8), however, a rapid positive increase of pitching moment with increasing sideslip indicates the possibility of cross coupling of the lateral, directional, and longitudinal motions. This cross-coupling tendency, combined with the greatly reduced directional stability, might be the source of undesirable stability characteristics at the high angles of attack.

#### Lateral and Directional Control

Aileron characteristics.- The effects of aileron deflection on the lateral aerodynamic characteristics at  $M = 1.61$  for the basic configuration are presented in figure 19. The aileron remains effective in producing roll throughout the angle-of-attack and angle-of-sideslip

ranges investigated. The results at  $\alpha = 0^\circ$  indicate that deflection of the left aileron provides larger increments of rolling moment and smaller increments of yawing moment at positive sideslip angles than at negative sideslip angles. This probably occurs because the flow over the left wing tends to become more subsonic at positive sideslip angles and less subsonic at negative sideslip angles. These increments of rolling and yawing moments may also be associated with interference effects at the tail; however, no aileron deflection tests were made with the tails removed.

Although the linearity of rolling moment with aileron deflection was not determined for deflections above about  $10^\circ$ , it appears that sufficient rolling power would be available to neutralize the maximum rolling moments encountered throughout the  $\alpha$  and  $\beta$  ranges investigated with the possible exception of some combinations of  $\alpha$  and  $\beta$  above  $\alpha \approx 12^\circ$  where  $C_{l\beta}$  becomes large (fig. 15).

The aileron effectiveness at  $\beta = 0^\circ$  appears to increase slightly with increasing angle of attack (fig. 21).

Upward deflections of the left aileron caused a negative yawing-moment increment at low angles of attack, whereas downward deflections caused negative yawing-moment increments at high angles of attack. Although these increments were small, they may, under the conditions of initially low directional stability and for greater aileron deflections, assume greater importance.

Deflection of the aileron does not appear to alter significantly the variation of  $C_L$ ,  $C_X$ , and  $C_m$  with  $\beta$  for angles of attack of  $0^\circ$  and  $8.3^\circ$  (fig. 20). At  $\alpha \approx 20.9^\circ$ , negative deflection of one aileron appears to result in a more rapid increase of  $C_m$  with  $\beta$  than for zero deflection. However, opposite deflection of the other aileron should reduce this effect. As expected, deflection of the left aileron produces slightly greater increments of lift and pitching moment at positive sideslip angles than at negative sideslip angles. The differences in drag increments due to aileron deflection at positive and negative sideslip angles ( $\alpha = 0^\circ$ ) were small.

Rudder characteristics.— A rudder deflection of  $10^\circ$  for the basic configuration at  $M = 1.61$  produces an essentially constant increment of  $C_n$ ,  $C_l$ , and  $C_y$  throughout the angle-of-attack and sideslip ranges (figs. 22 and 24). At an angle of attack of  $0^\circ$ , a rudder deflection of  $10^\circ$  provides a trimmed sideslip angle of  $2^\circ$ . The trimmed sideslip angles increase with increasing angle of attack as the directional stability decreases until the trimmed angles would become infinite and then reverse in sign as the configuration becomes directionally unstable.

It is apparent that, because of the nonlinear variation of  $C_n$  with  $\beta$ , large deflections of the rudder might increase the tendency toward yawing divergence.

A rudder deflection of  $10^\circ$  resulted in small decreases in lift and slight positive increases in pitching moments for all angles of attack (fig. 23).

### CONCLUSIONS

An investigation has been made in the Langley 4- by 4-foot supersonic pressure tunnel at Mach numbers of 1.41, 1.61, and 2.01 to determine the static lateral stability and control characteristics of a model of a  $45^\circ$  swept-wing fighter airplane equipped with various vertical tails. The results of the investigation indicated the following conclusions:

1. Because of the loss in vertical-tail lift-curve slope and because of the magnitude of the unstable wing-body moment, the directional stability derivative  $C_{n\beta}$  for the complete configuration progressively decreased with increasing Mach number and increasing angle of attack until regions of directional instability occurred.
2. Increasing the size of the vertical tail provided positive increases in  $C_{n\beta}$  so that the onset of directional instability was delayed to higher Mach numbers or higher angles of attack.
3. The lateral control provided by the ailerons and the directional control provided by the rudder at a Mach number of 1.61 were essentially constant throughout the angle-of-attack and sideslip ranges.

Langley Aeronautical Laboratory,  
National Advisory Committee for Aeronautics,  
Langley Field, Va., March 28, 1956.

~~REFERENCES~~

1. Driver, Cornelius, and Foster, Gerald V.: Static Longitudinal Stability and Control Characteristics of a Model of a  $45^\circ$  Swept-Wing Fighter Airplane at Mach Numbers of 1.41, 1.61, and 2.01. NACA RM L56D04, 1956.
2. Drake, Hubert M., Finch, Thomas W., and Peele, James R.: Flight Measurements of Directional Stability to a Mach Number of 1.48 for an Airplane Tested With Three Different Vertical Tail Configurations. NACA RM H55G26, 1955.
3. Robinson, Ross B.: Longitudinal Characteristics of an Unswept-Wing Fighter-Type Model With External Stores at a Mach Number of 1.82 and Some Effects of Horizontal-Tail and Yaw-Damper Deflection on the Sideslip Derivatives. NACA RM L55L26, 1956.
4. Jones, Arthur L., Sprieter, John R., and Alksne, Alberta: The Rolling Moment Due to Sideslip of Triangular, Trapezoid, and Related Plan Forms in Supersonic Flow. NACA TN 1700, 1948.

TABLE I

## GEOMETRIC CHARACTERISTICS OF THE MODEL

## Wing:

Area, sq ft . . . . .	1.89
Span, in. . . . .	32.41
Aspect ratio . . . . .	3.86
Taper ratio . . . . .	0.262
Mean geometric chord, in. . . . .	9.38
Sweep of 0.25c line, deg . . . . .	45
Incidence, deg . . . . .	0
Dihedral, deg . . . . .	0
Twist, deg . . . . .	0
Airfoil section . . . . .	NACA 64(06)A007
Aileron area, sq in. . . . .	13.60

## Fuselage:

Length, in. . . . .	40.45
Frontal area, sq ft . . . . .	0.13

## Horizontal tail:

Area, sq ft . . . . .	0.48
Span, in. . . . .	15.73
Aspect ratio . . . . .	3.54
Taper ratio . . . . .	0.302
Mean geometric chord, in. . . . .	4.88
Sweep of 0.25c line, deg . . . . .	45
Airfoil section . . . . .	NACA 65A003.5
Tail length, 0.25c of wing to 0.25c of horizontal tail, in. . . . .	12.07

## Vertical tails:

	Basic	Extended tip	127-percent modification
Area, sq ft . . . . .	0.167	0.190	0.213
Span (exposed), in. . . . .	5.16	6.62	6.66
Aspect ratio . . . . .	1.10	1.61	1.45
Taper ratio . . . . .	0.428	0.267	0.301
Sweep of 0.25c line, deg . . . . .	45	45	45
Airfoil section (all verticals) . . . . .	NACA 65A003.5		

TABLE II.- INDEX OF FIGURES

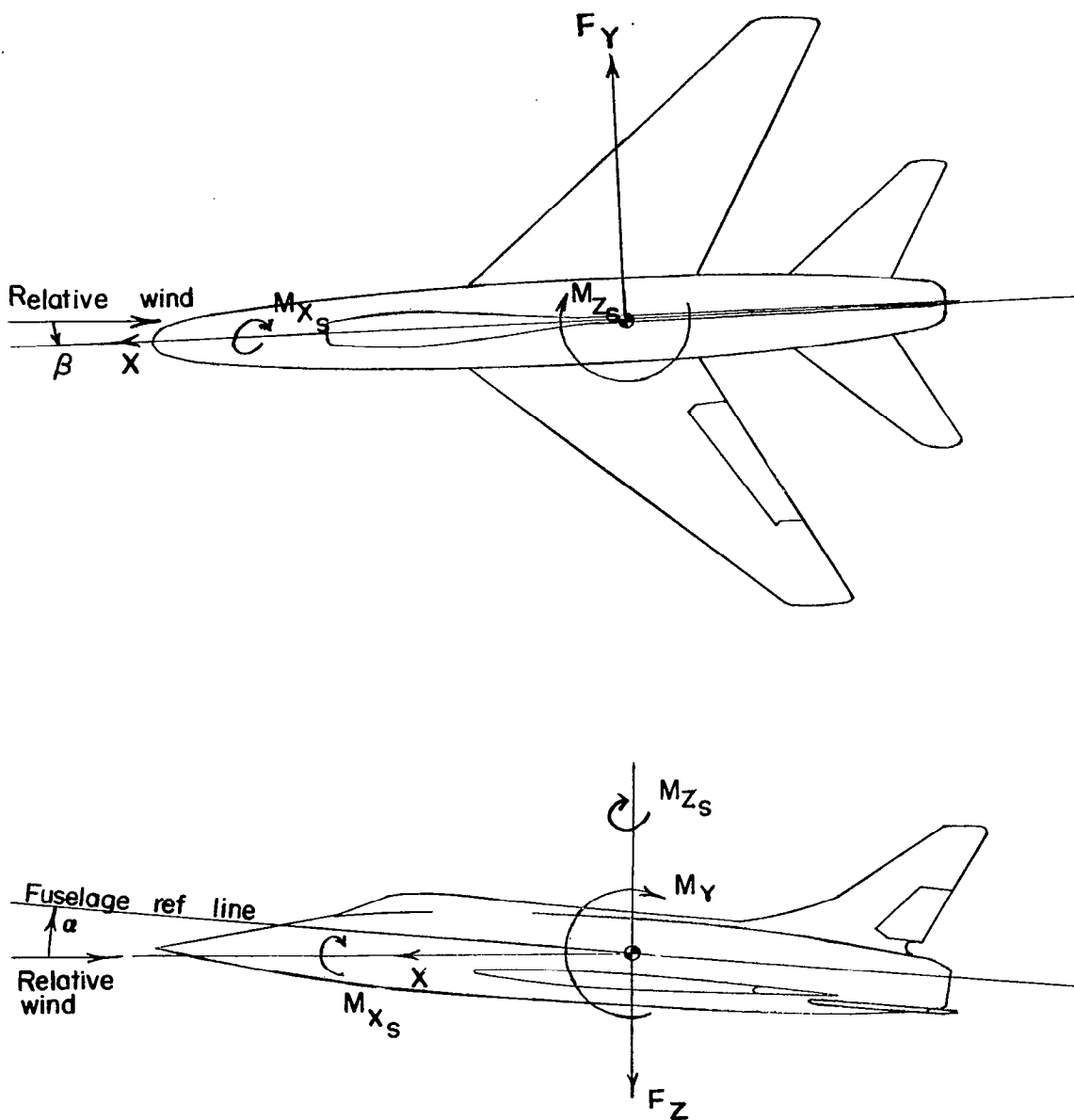
Figure	M	V	H	$i_t$ , deg	$\delta_a$ , deg		$\delta_r$ , deg	$\alpha$ , deg	$\beta$ , deg	Component	Type of data
					Left	Right					
4	1.41	Basic	On	0	0	0	0	5.1	Range	$C_n, C_l, C_Y, C_m, C_X, C_L$	Basic data
		127-percent modification	On	0	0	0	0	5.1	Range	$C_n, C_l, C_Y, C_m, C_X, C_L$	Basic data
		Off	On	0	0	0	0	5.1	Range	$C_n, C_l, C_Y, C_m, C_X, C_L$	Basic data
5	1.41	Basic	On	0	0	0	0	Range	-4.8	$C_n, C_l, C_Y$	Basic data
		127-percent modification	On	0	0	0	0	Range	-4.8	$C_n, C_l, C_Y$	Basic data
6	1.61	Basic	On	0	0	0	0	0, 8.3, 15.7, 20.9	Range	$C_n, C_l, C_Y$	Basic data
		Basic	Off	-	0	0	0	0, 8.3, 15.7, 20.9	Range	$C_n, C_l, C_Y$	Basic data
		Off	Off	-	0	0	-	0, 8.3, 15.7, 20.9	Range	$C_n, C_l, C_Y$	Basic data
		Off	On	0	0	0	-	0, 8.3, 15.7, 20.9	Range	$C_n, C_l, C_Y$	Basic data
7	1.61	Basic	On	0	0	0	0	0, 4.1, 8.3, 15.7, 20.9	Range	$C_n, C_l, C_Y$	Basic data
		Extended tip	On	0	0	0	0	0, 4.1 8.3, 15.7	Range	$C_n, C_l, C_Y$	Basic data
		127-percent modification	On	0	0	0	0	0, 8.3, 15.7, 20.9	Range	$C_n, C_l, C_Y$	Basic data
		Off	On	0	0	0	-	0, 8.3, 15.7, 20.9	Range	$C_n, C_l, C_Y$	Basic data
		Off	Off	-	0	0	-	0, 8.3, 15.7, 20.9	Range	$C_n, C_l, C_Y$	Basic data
8	1.61	Basic	On	0	0	0	0	0, 4.1, 8.3, 15.7, 20.9	Range	$C_L, C_X, C_m$	Basic data
		Extended tip	On	0	0	0	0	0, 4.1, 8.3, 15.7	Range	$C_L, C_X, C_m$	Basic data
		127-percent modification	On	0	0	0	0	0, 8.3, 15.7, 20.9	Range	$C_L, C_X, C_m$	Basic data
9	1.61	Basic	On	0, -5, -10	0	0	0	0, 8.3, 20.9	Range	$C_n, C_l, C_Y$	Basic data
		Off	On	0, -10	0	0	-	0, 8.3, 15.7, 20.9	Range	$C_n, C_l, C_Y$	Basic data

TABLE II.- INDEX OF FIGURES - Concluded

Figure	M	V	H	$i_t$ , deg	$\delta_a$ , deg		$\delta_r$ , deg	$\alpha$ , deg	$\beta$ , deg	Component	Type of data
					Left	Right					
10	2.01	Basic	On	0, -10	0	0	0	0, 4.1, 8.2	Range	$C_n, C_l, C_Y$	Basic data
		Basic	Off	-----	0	0	0	0, 4.1, 8.2	Range	$C_n, C_l, C_Y$	Basic data
		Off	Off	-----	0	0	-----	0, 4.1, 8.2	Range	$C_n, C_l, C_Y$	Basic data
		Off	On	0	0	0	-----	0, 4.1, 8.2	Range	$C_n, C_l, C_Y$	Basic data
11	2.01	Basic	On	0	0	0	0	0, 4.1, 8.2	Range	$C_L, C_X, C_m$	Basic data
12	1.41	Various	On	0	0	0	0	Range	-----	$C_{n\beta}, C_{l\beta}, C_{Y\beta}$	Summary data
13	1.61	Various	On and off	0	0	0	0	Range	-----	$C_{n\beta}, C_{l\beta}, C_{Y\beta}$	Summary data
14	2.01	Basic	On and off	0	0	0	0	Range	-----	$C_{n\beta}, C_{l\beta}, C_{Y\beta}$	Summary data
15	Various	Basic	On	0	0	0	0	Range	-----	$C_{n\beta}, C_{l\beta}, C_{Y\beta}$	Summary data
16	Various	Off	Off	-----	0	0	-----	Range	-----	$C_{n\beta}, C_{l\beta}, C_{Y\beta}$	Summary data
17	Various	Various	On and off	0	0	0	0	0	-----	$C_{n\beta}, C_{l\beta}, C_{Y\beta}$	Summary data
18	1.61	Basic, on and off	On and off	0	0	0	0	Range	-----	$C_{n\beta}$	Summary data; body and stability axes
19	1.61	Basic	On	0	-10.8, 0, 9.9	0	0	0, 8.3, 20.9	Range	$C_n, C_l, C_Y$	Aileron control
20	1.61	Basic	On	0	-10.8, 0, 9.9	0	0	0, 8.3, 20.9	Range	$C_L, C_X, C_m$	Aileron control
21	1.61	Basic	On	0	-10.8, 0, 9.9	0	0	Range	0	$C_n, C_l, C_Y$	Aileron control
22	1.61	Basic	On	0	0	0	0, 10	0, 8.3, 20.9	Range	$C_n, C_l, C_Y$	Rudder control
23	1.61	Basic	On	0	0	0	0, 10	0, 8.3, 20.9	Range	$C_L, C_X, C_m$	Rudder control
24	1.61	Basic	On	0	0	0	0, 10	Range	0	$C_n, C_l, C_Y$	Rudder control

CONFIDENTIAL

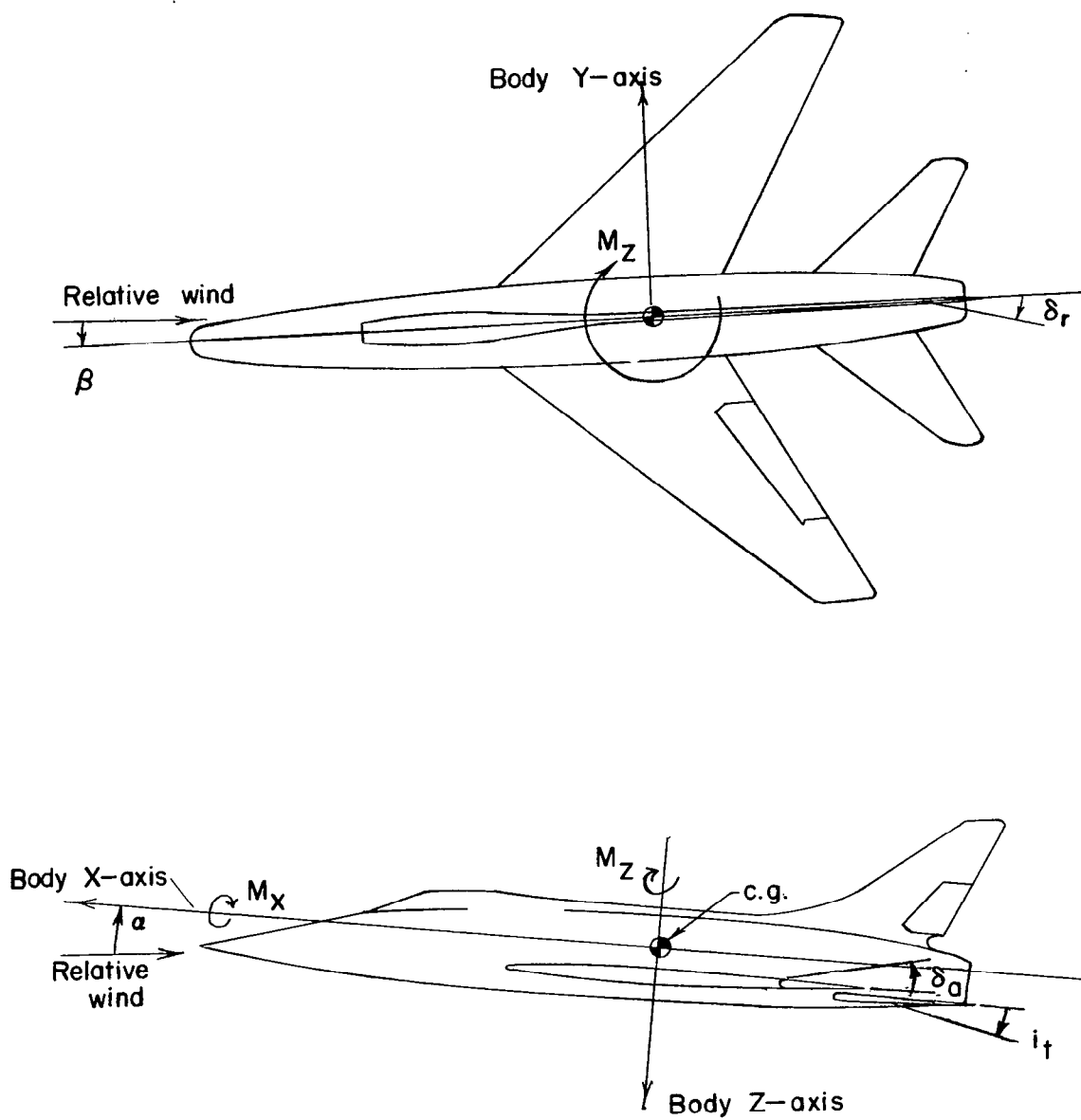
CONFIDENTIAL



(a) Stability axis system.

Figure 1.- Axis systems. Arrows indicate positive directions.





(b) Body axis system.

Figure 1.- Concluded.

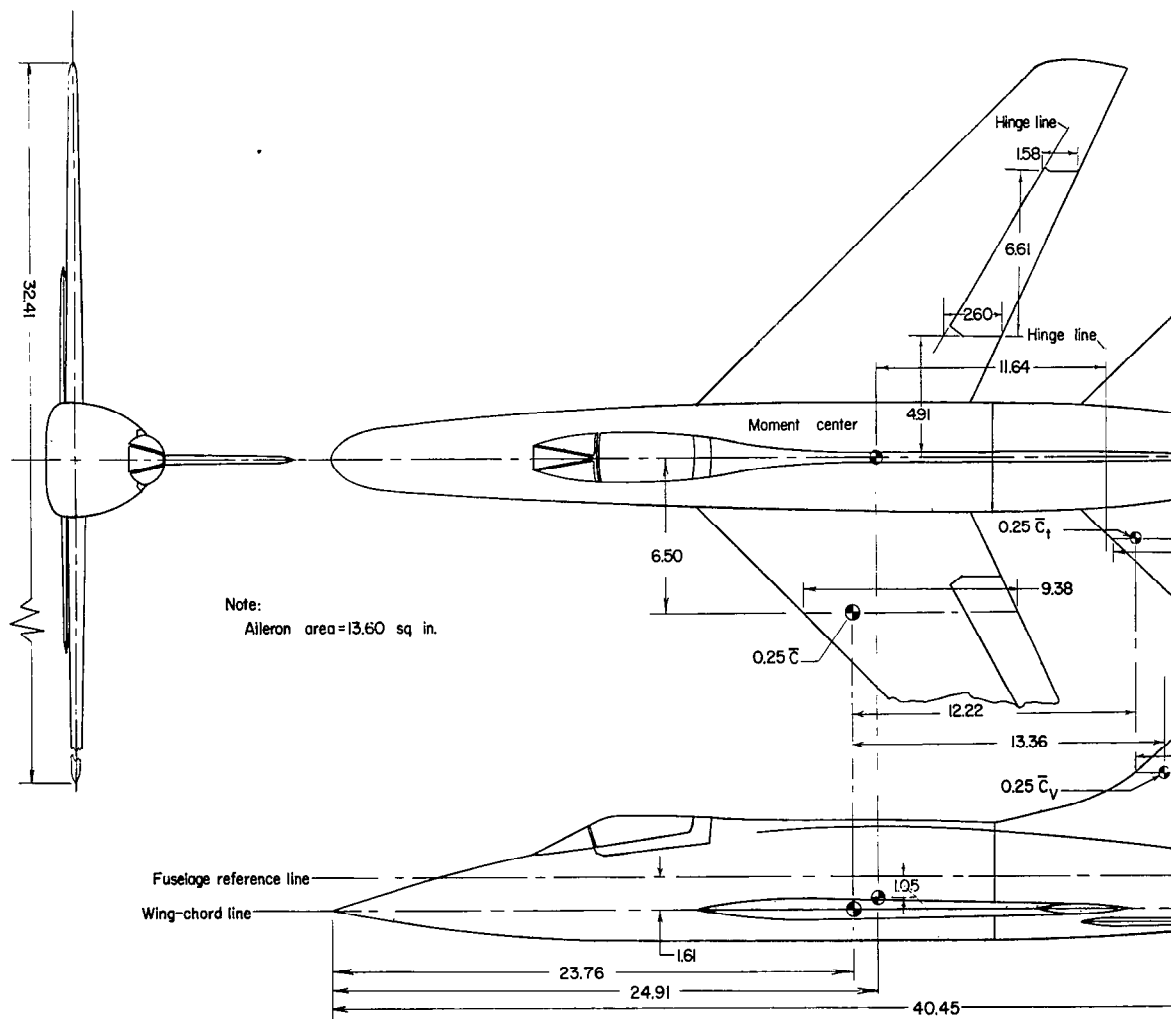


Figure 2.- Details of model.

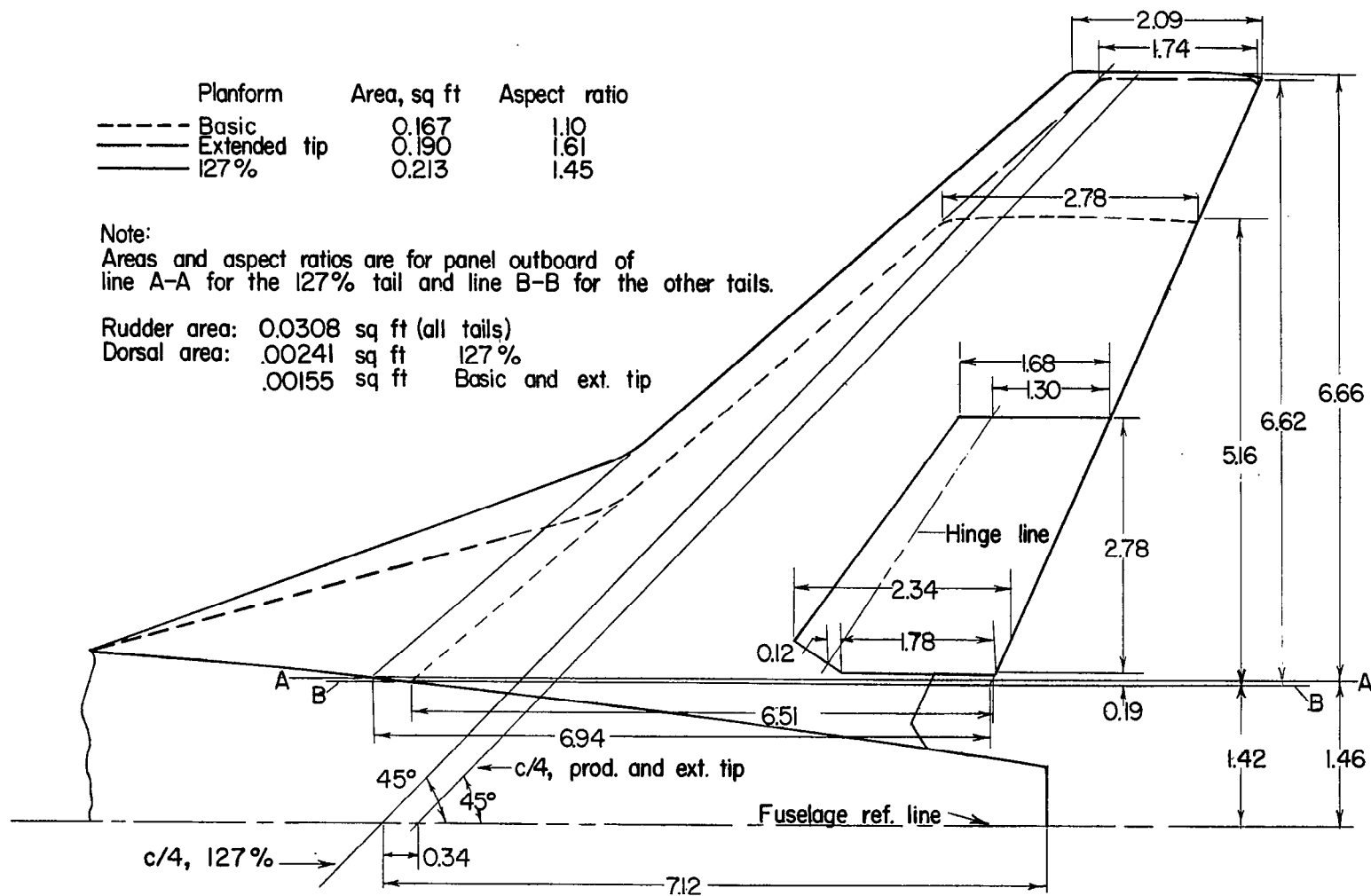


Figure 3.- Details of vertical tails.

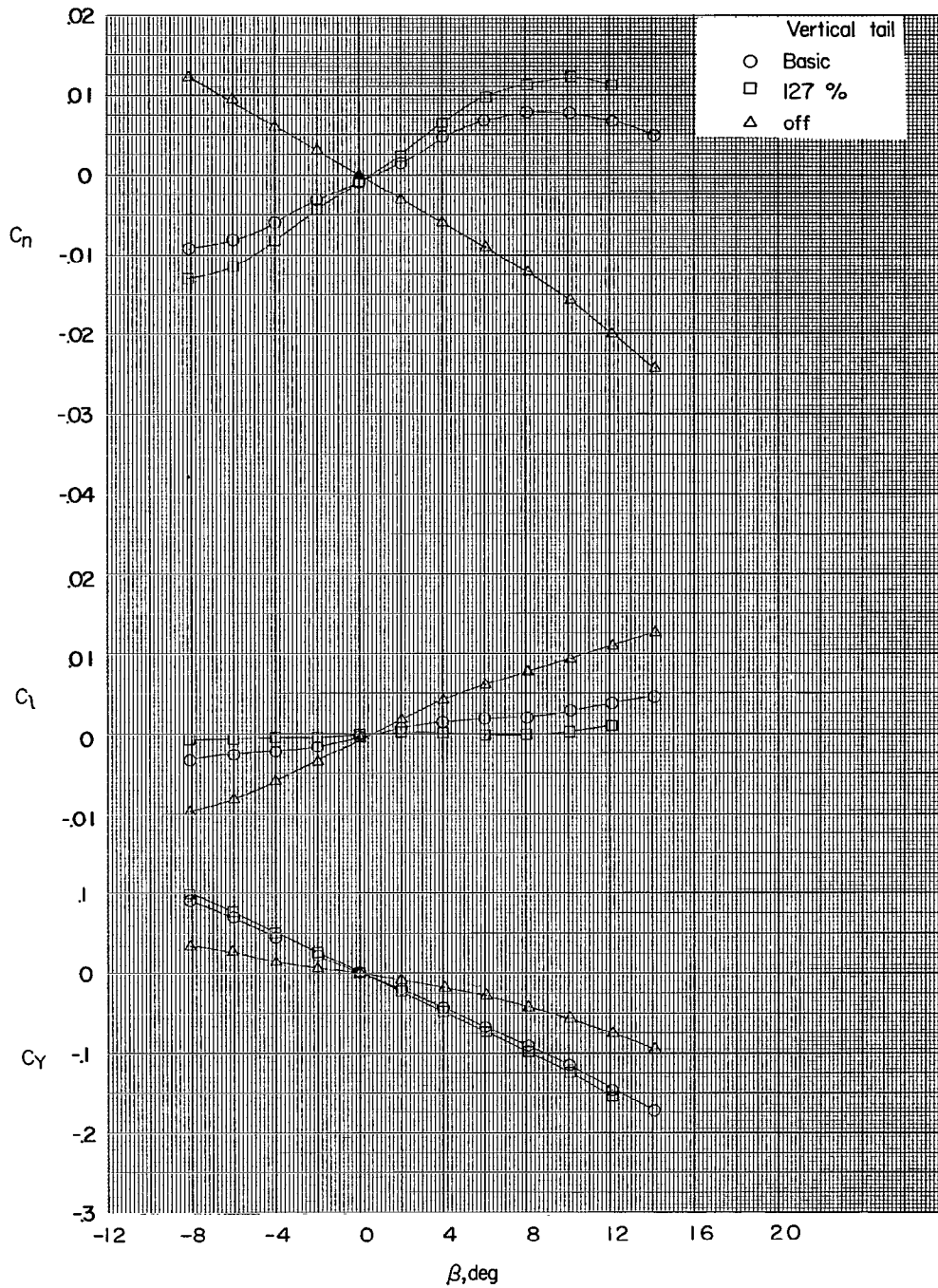


Figure 4.- Aerodynamic characteristics in sideslip.  $i_t = 0^\circ$ ;  $\alpha = 5.1^\circ$ ;  
 $M = 1.41$ .

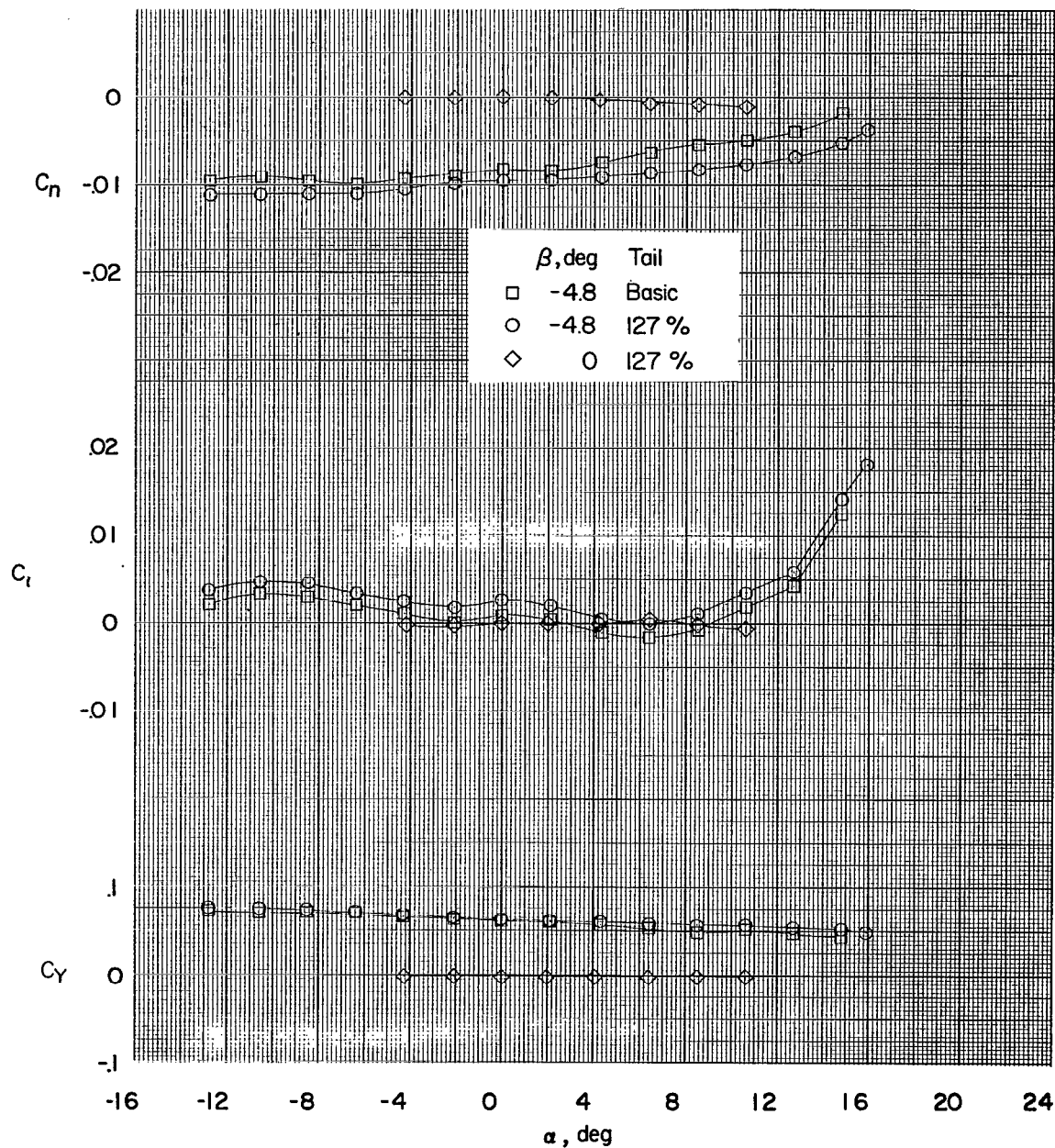


Figure 5.- Effect of angle of attack on lateral stability characteristics.  
 $M = 1.41$ .

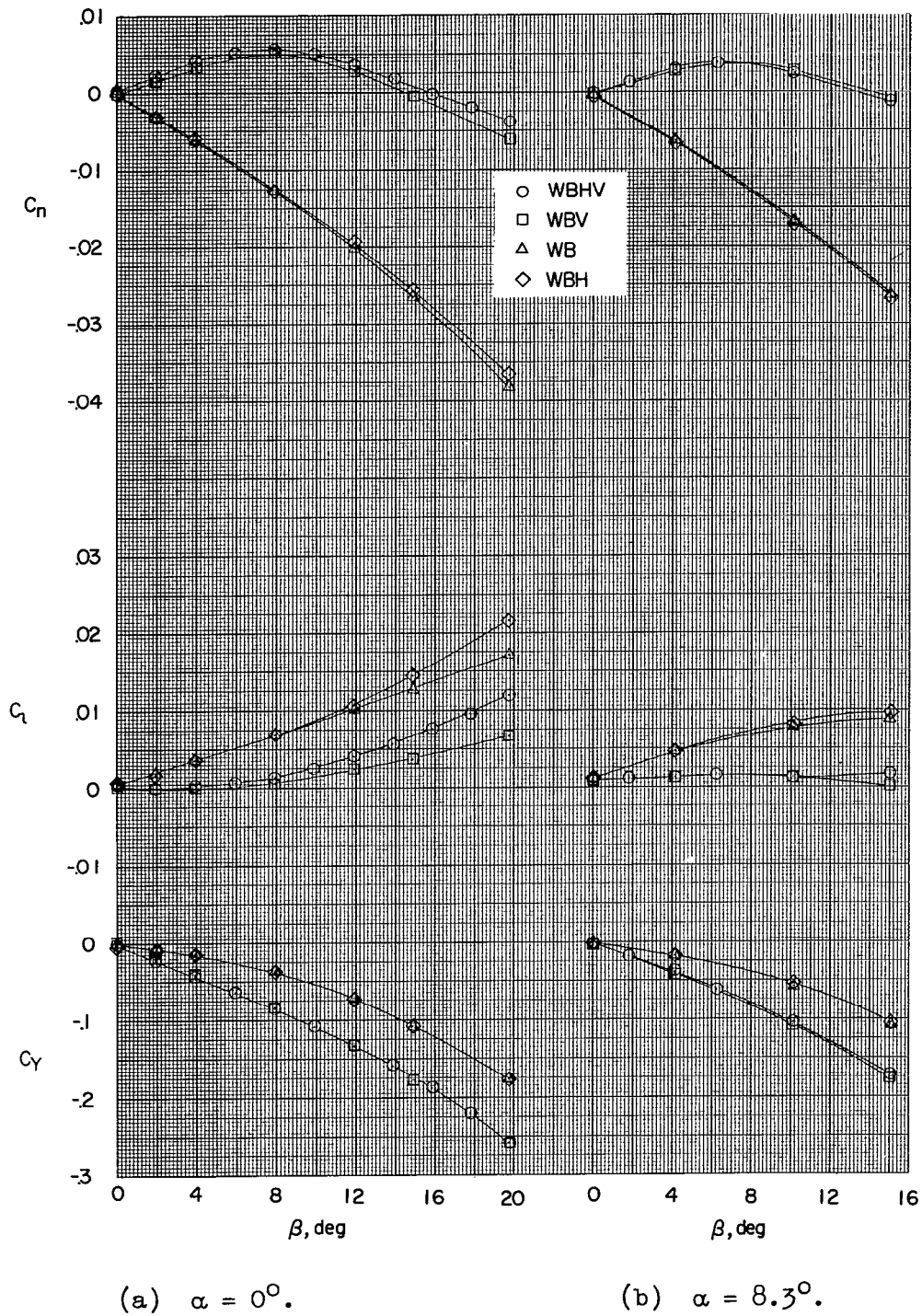


Figure 6.- Effect of component parts on aerodynamic characteristics in sideslip for various angles of attack. Basic tail;  $i_t = 0^\circ$ ;  $M = 1.61$ .

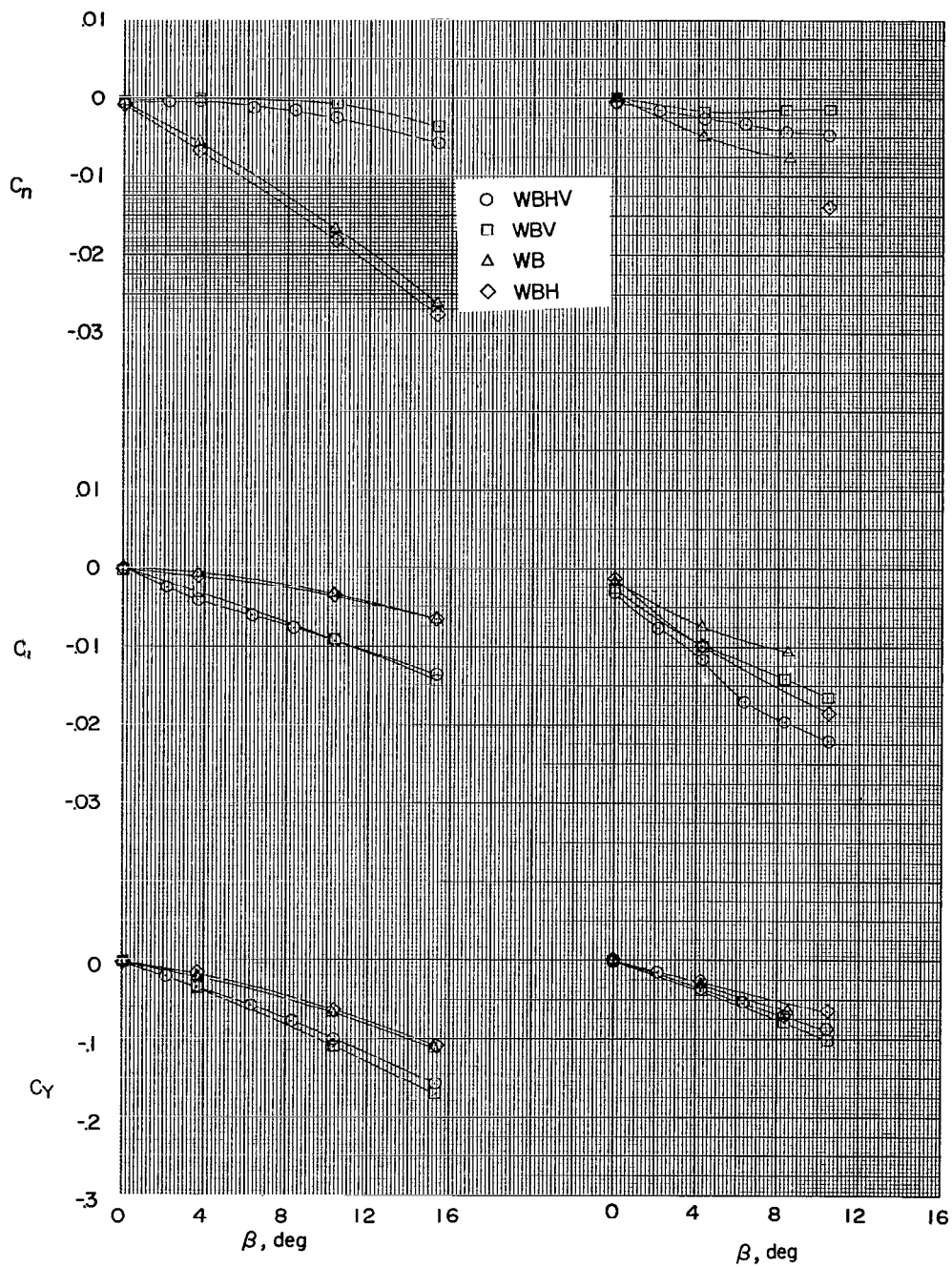


Figure 6.- Concluded.

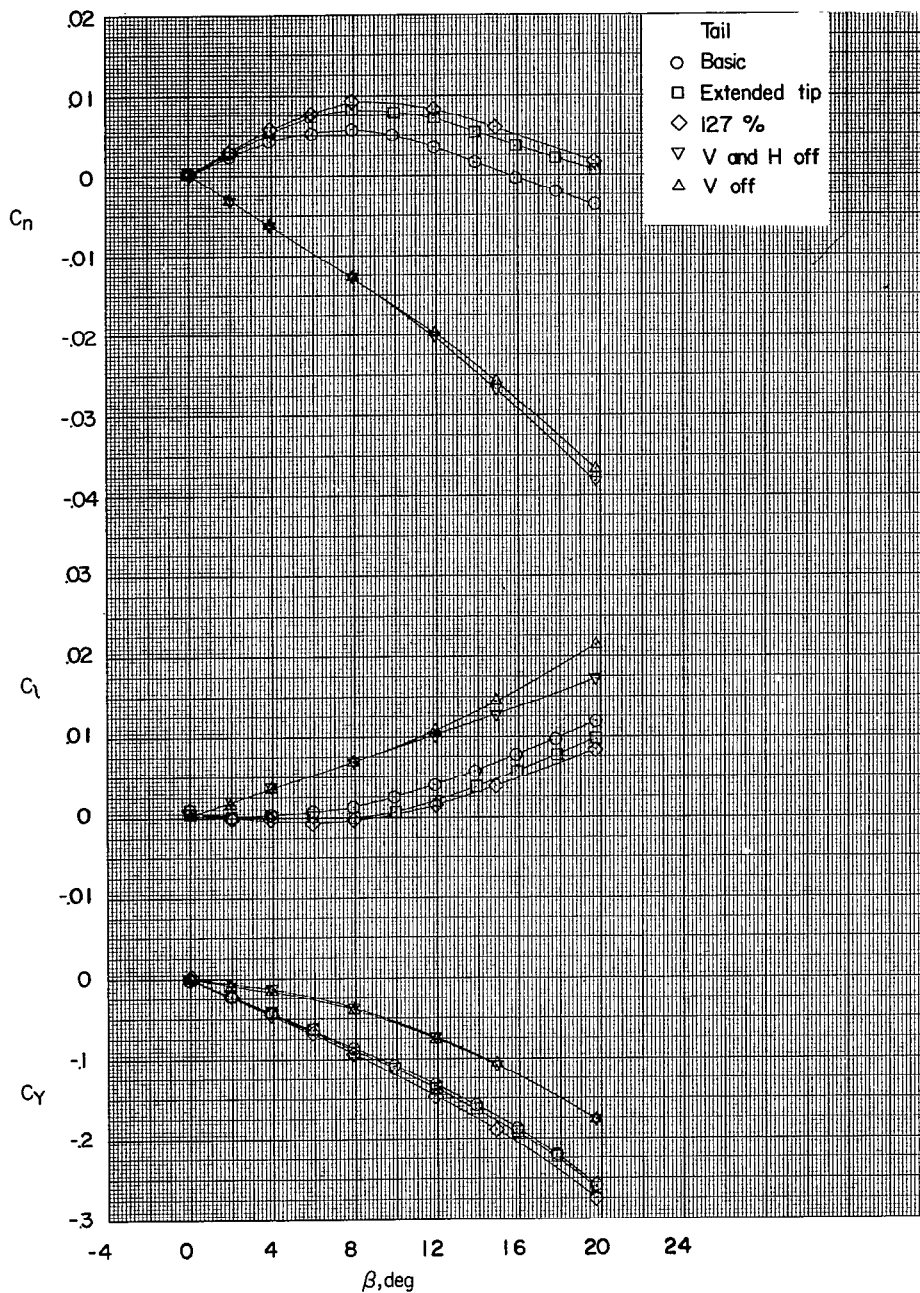
(a)  $\alpha = 0^\circ$ .

Figure 7.- Aerodynamic characteristics in sideslip for various tails and various angles of attack.  $i_t = 0^\circ$ ;  $M = 1.61$ .



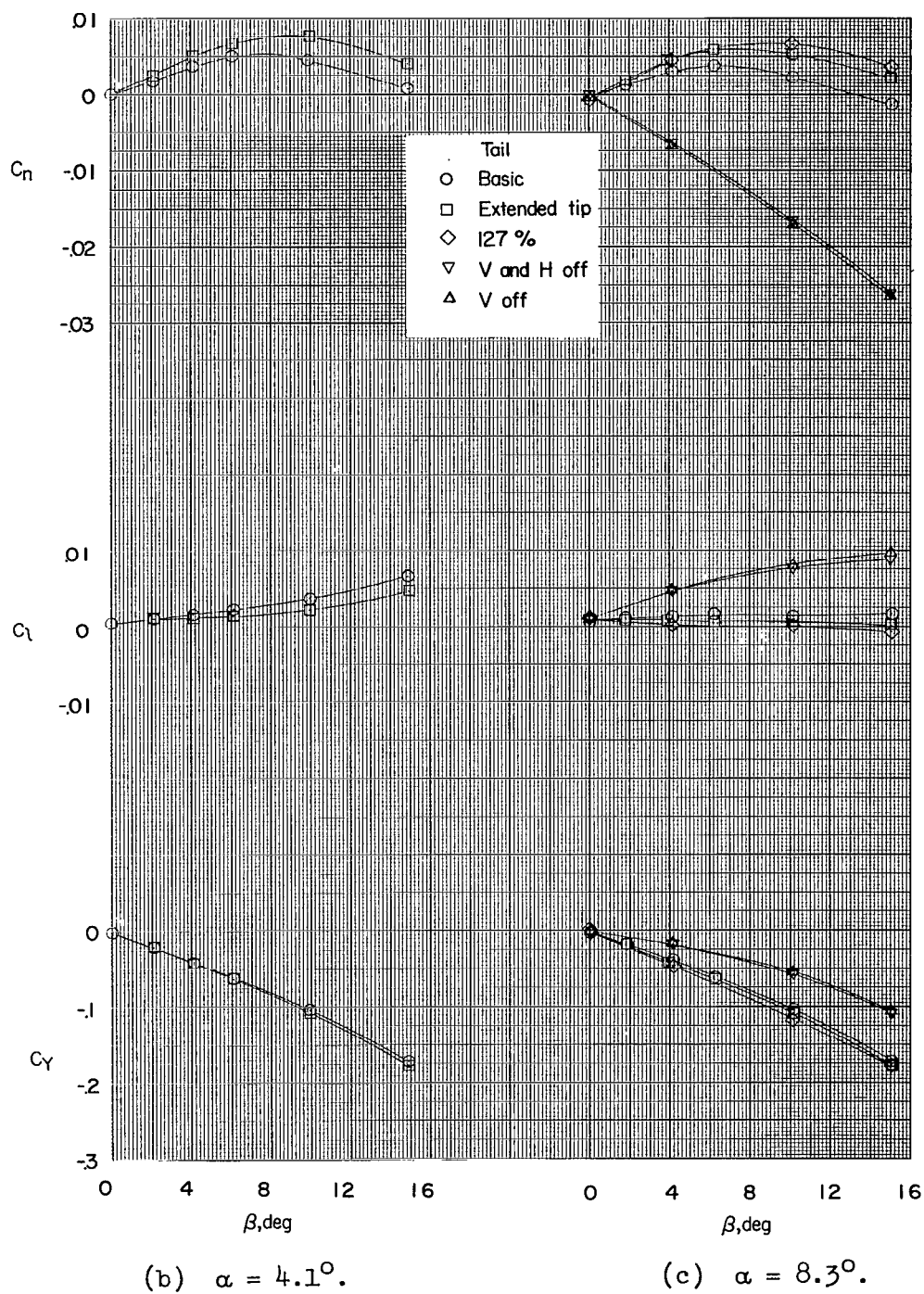


Figure 7.- Continued.

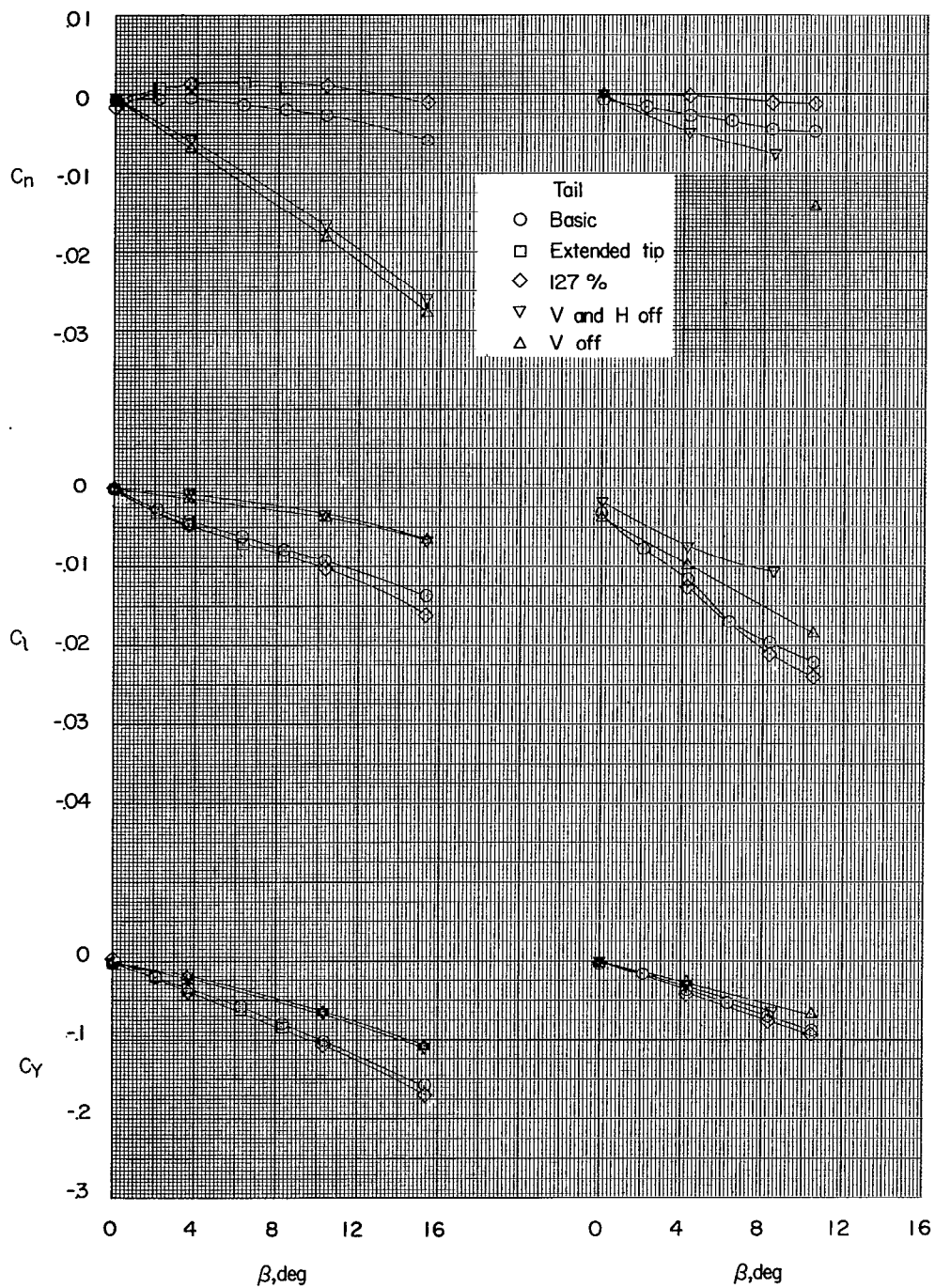
(d)  $\alpha = 15.7^\circ$ .(e)  $\alpha = 20.9^\circ$ .

Figure 7.- Concluded.

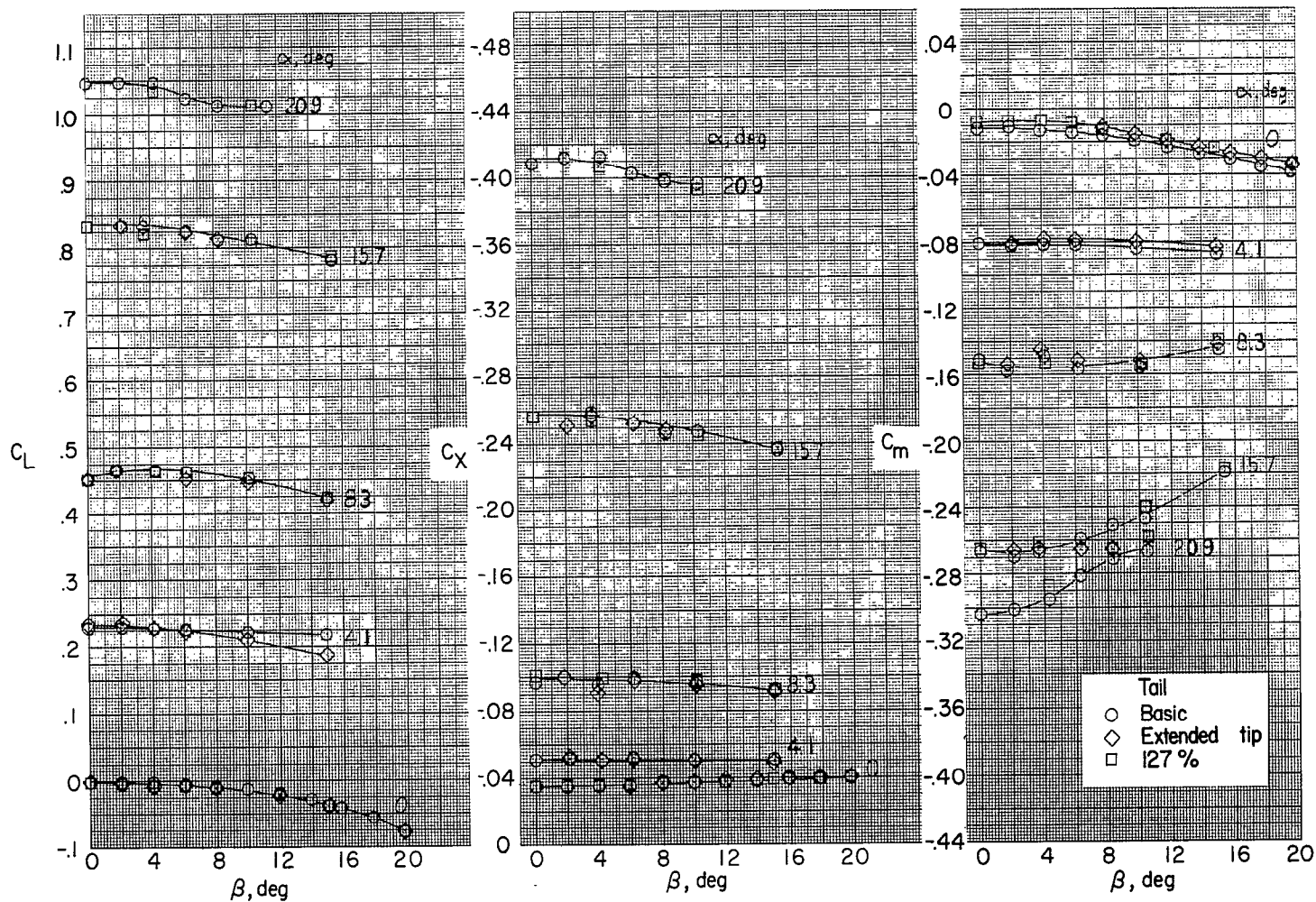


Figure 8.- Variation of lift, longitudinal-force, and pitching-moment coefficients with angle of sideslip for various angles of attack.  $M = 1.61$ .

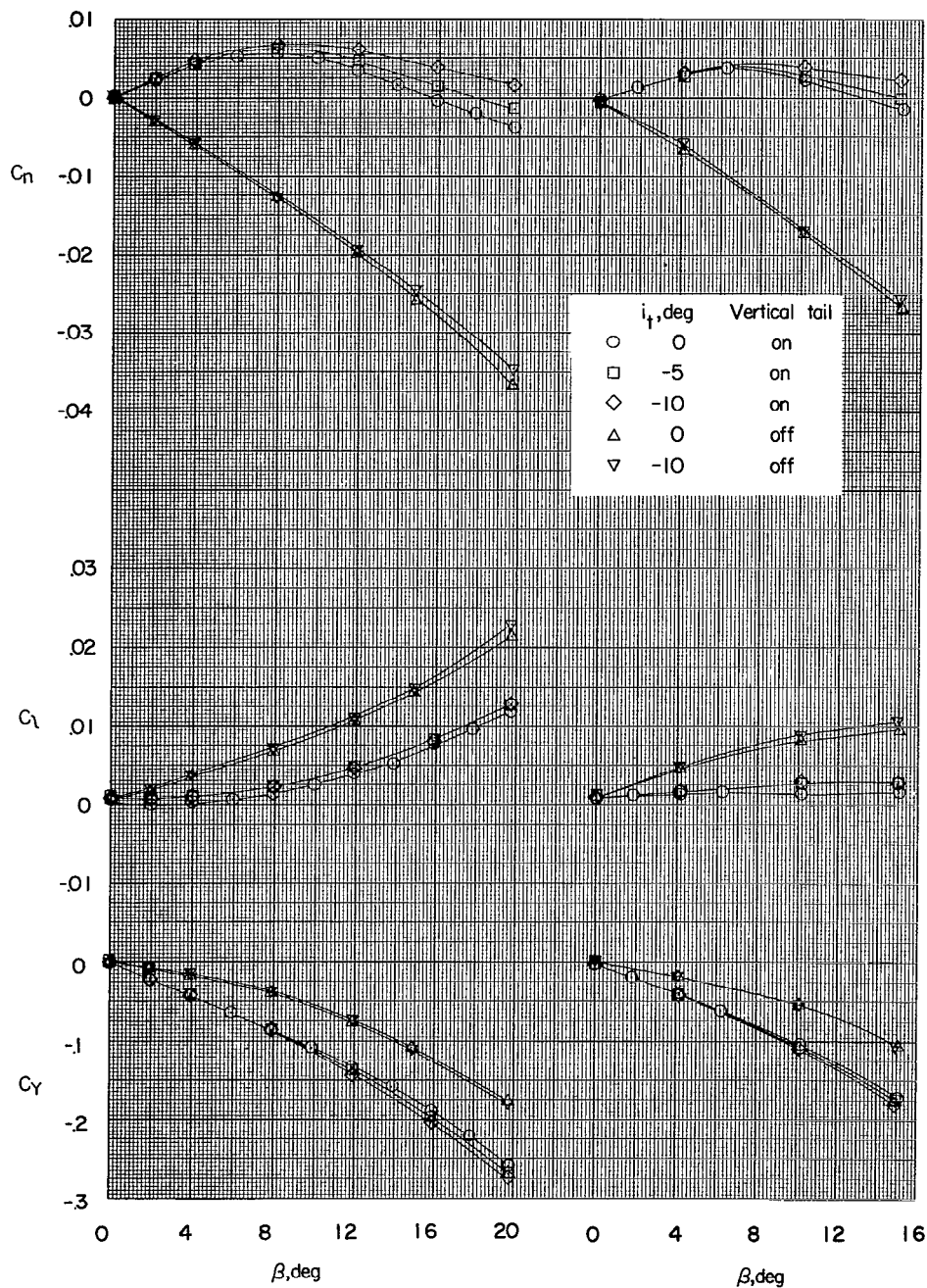
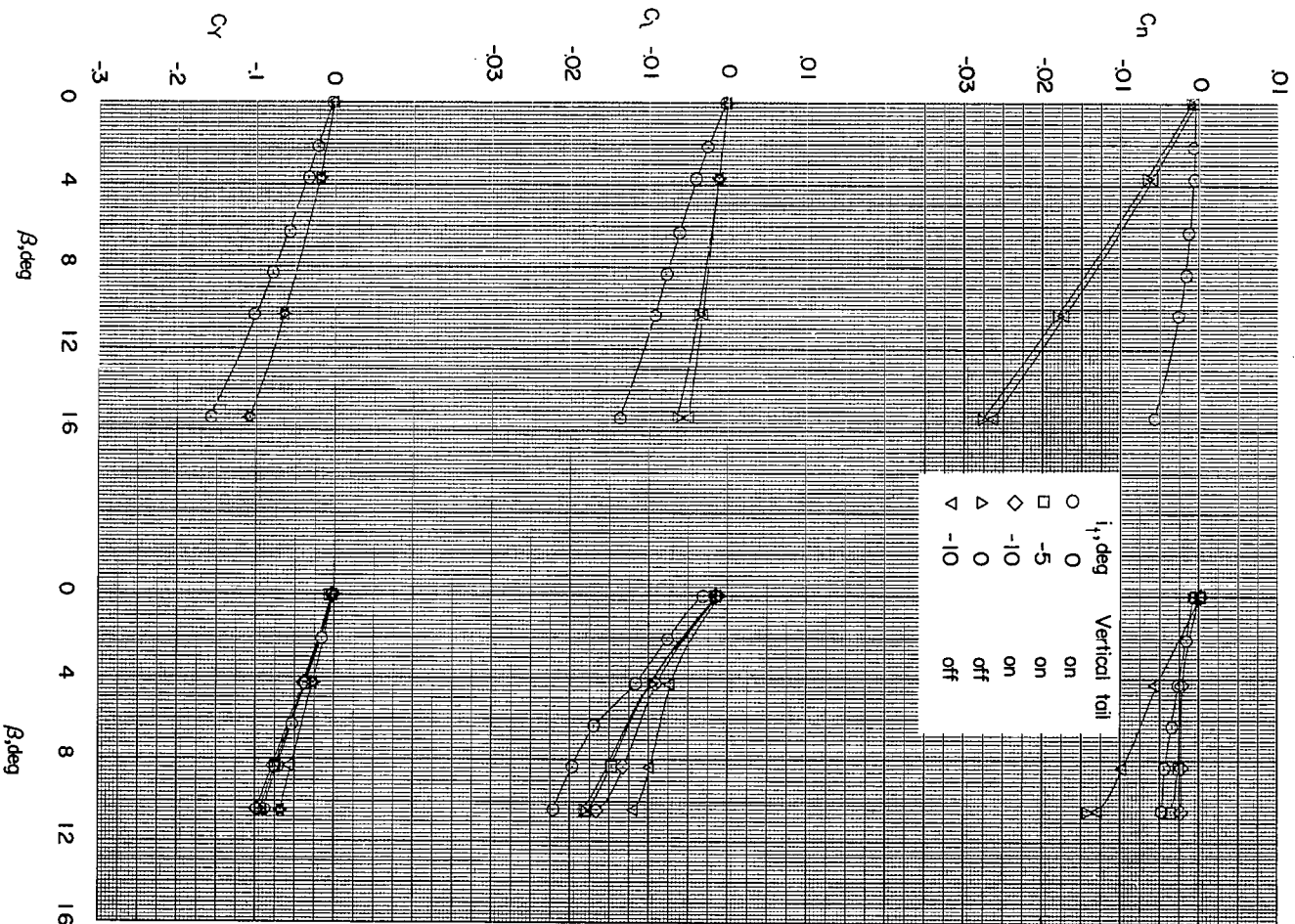
(a)  $\alpha = 0^\circ$ .(b)  $\alpha = 8.3^\circ$ .

Figure 9.- Effect of stabilizer deflection on aerodynamic characteristics in sideslip for various angles of attack. Basic tail;  $M = 1.61$ .



(c)  $\alpha = 15.7^\circ$ .

(d)  $\alpha = 20.9^\circ$ .

Figure 9.- Concluded.

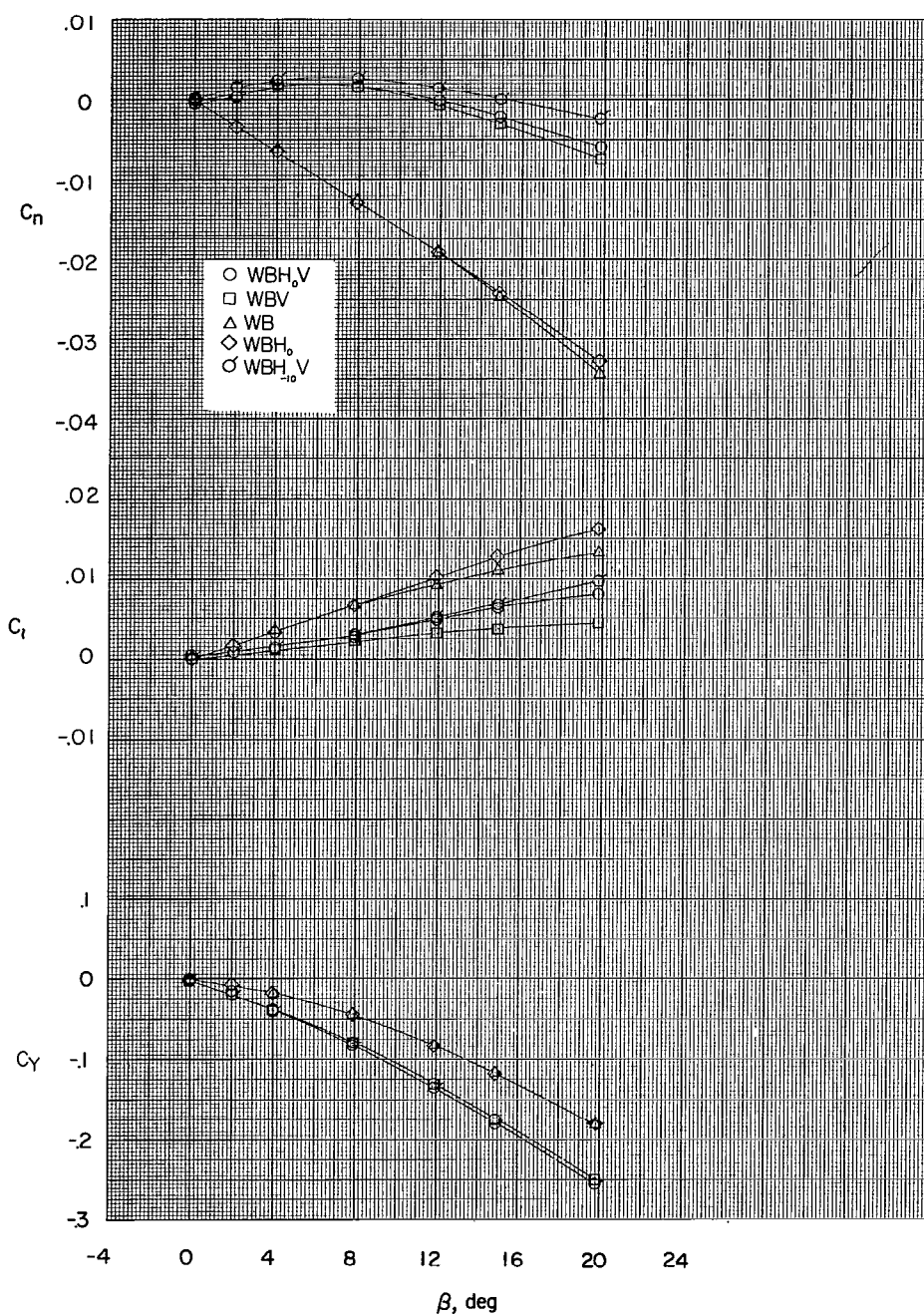
(a)  $\alpha = 0^\circ$ .

Figure 10.- Aerodynamic characteristics in sideslip at various angles of attack. Basic tail;  $M = 2.01$ .



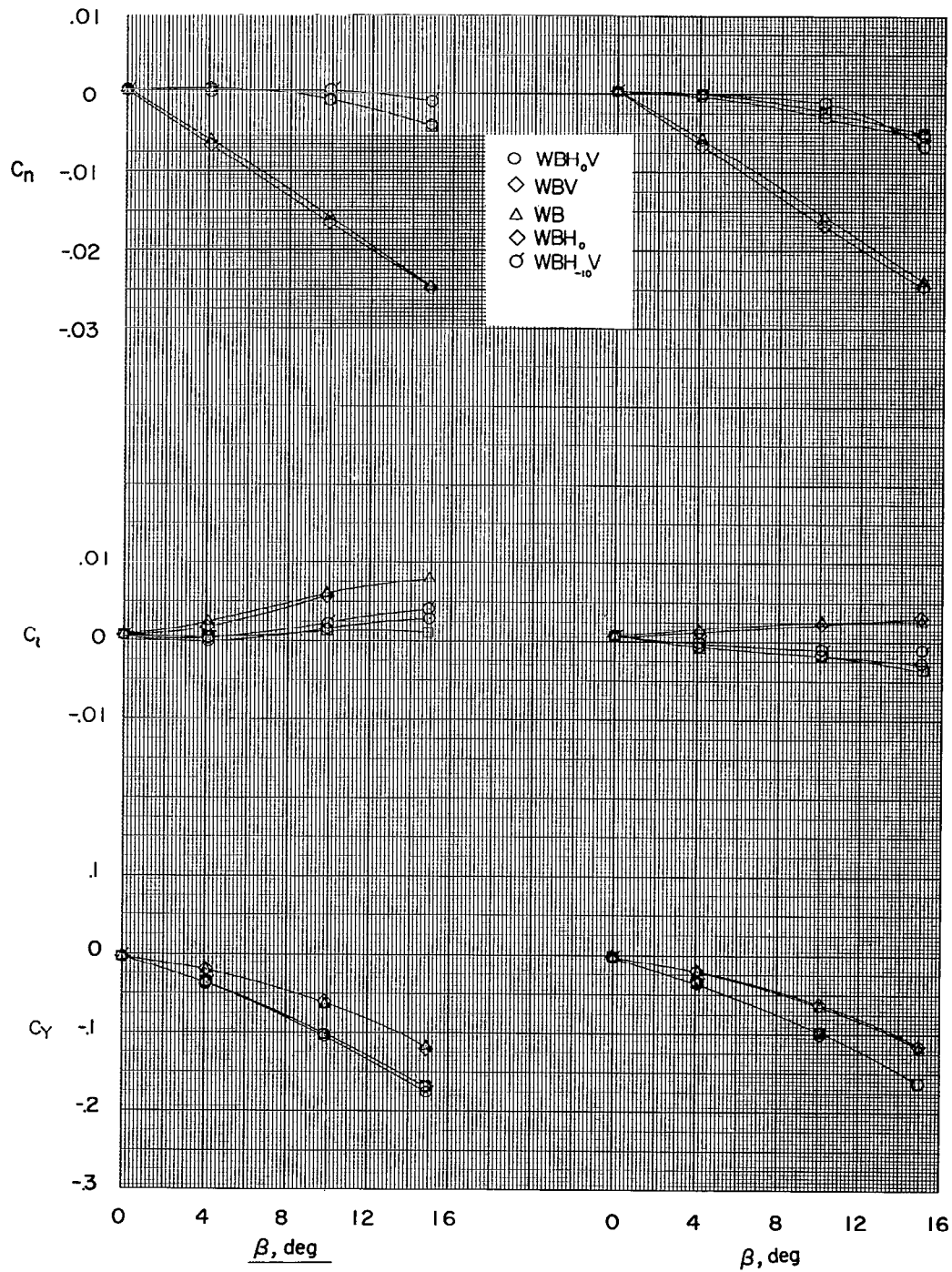
(b)  $\alpha = 4.1^\circ$ .(c)  $\alpha = 8.2^\circ$ .

Figure 10.- Concluded.

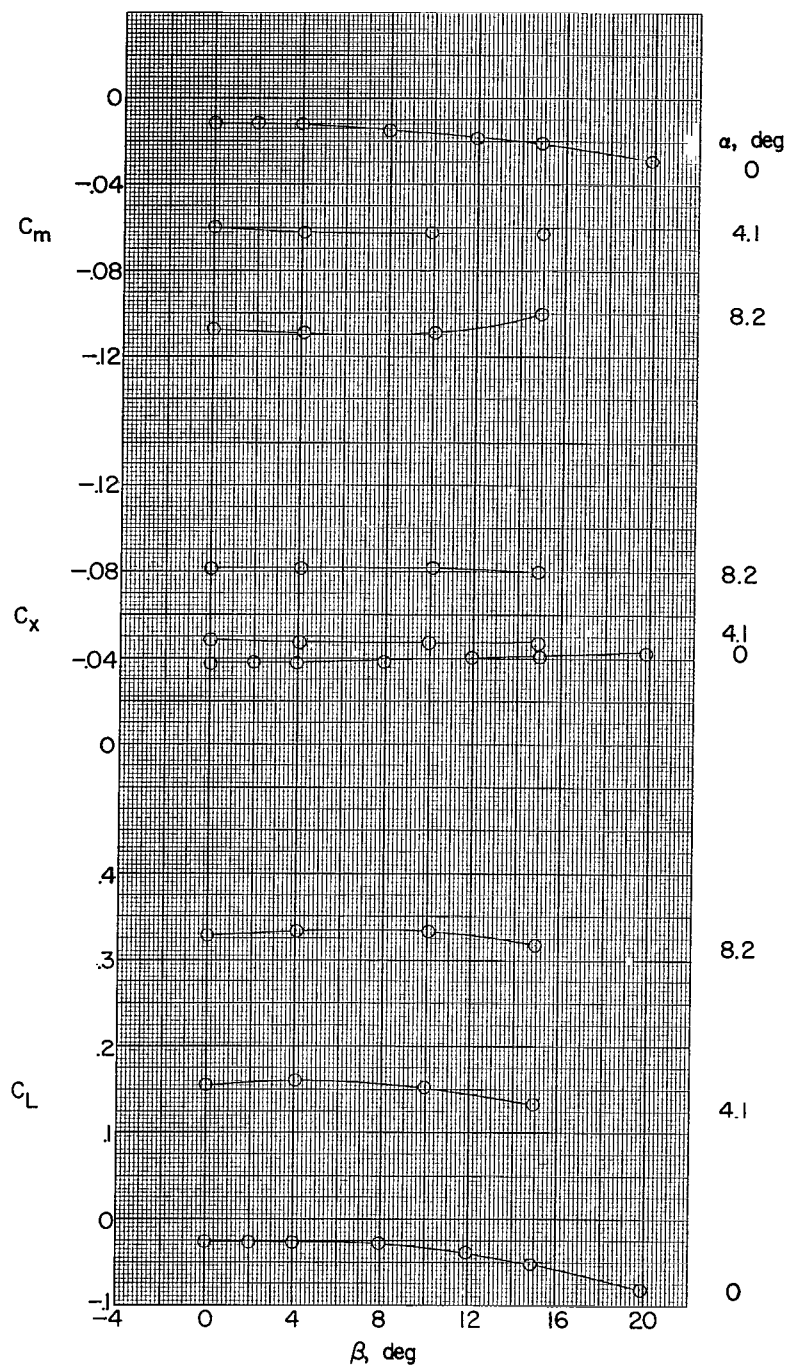


Figure 11.- Variation of lift, longitudinal-force, and pitching-moment coefficients with sideslip for various angles of attack. Complete model; basic tail;  $i_t = 0^\circ$ ;  $M = 2.01$ .



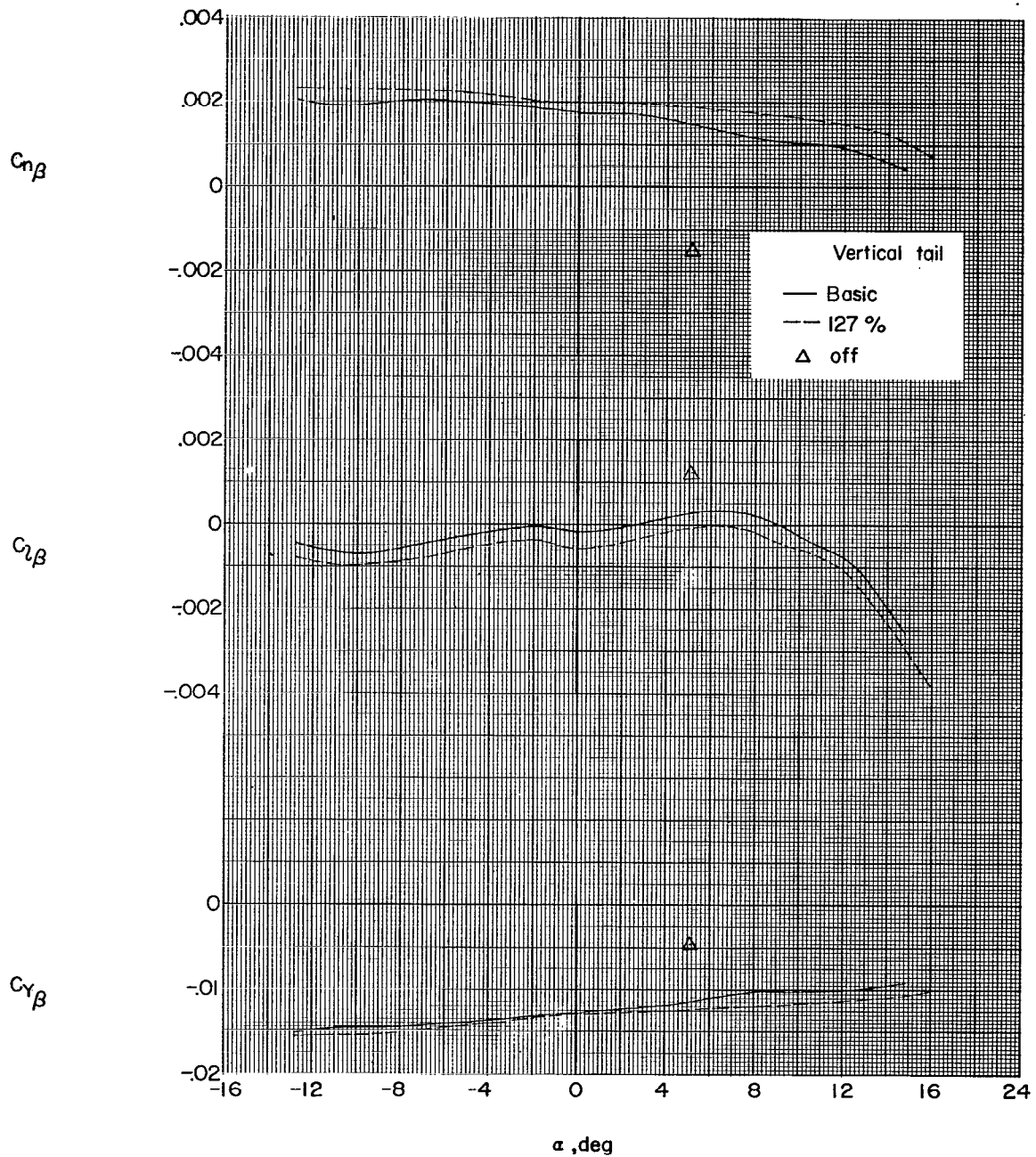


Figure 12.- Variation of sideslip derivatives with angle of attack.  
 $M = 1.41$ ; horizontal tail on.

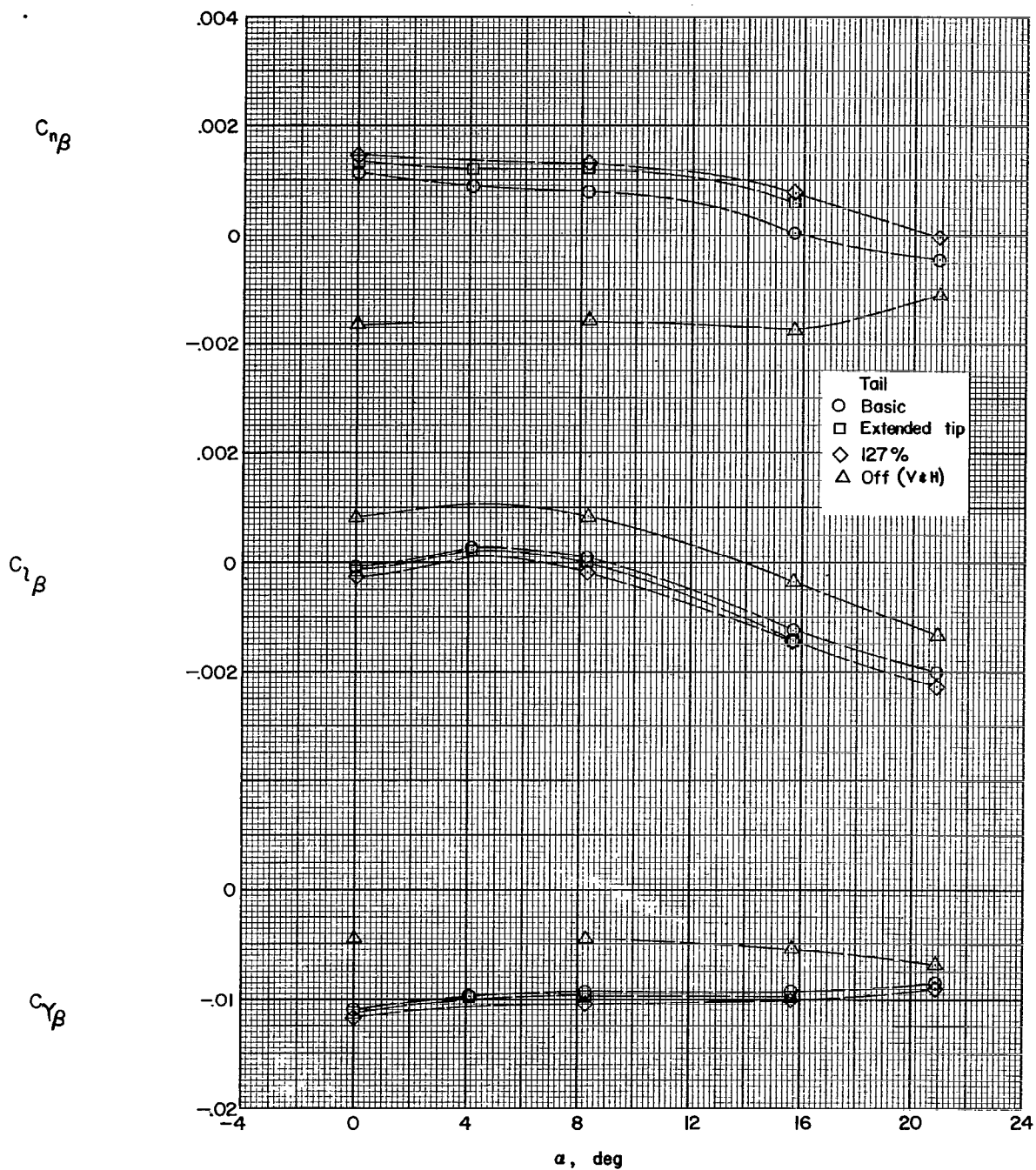


Figure 13.- Variation of sideslip derivatives with angle of attack.  
 $M = 1.61$ .

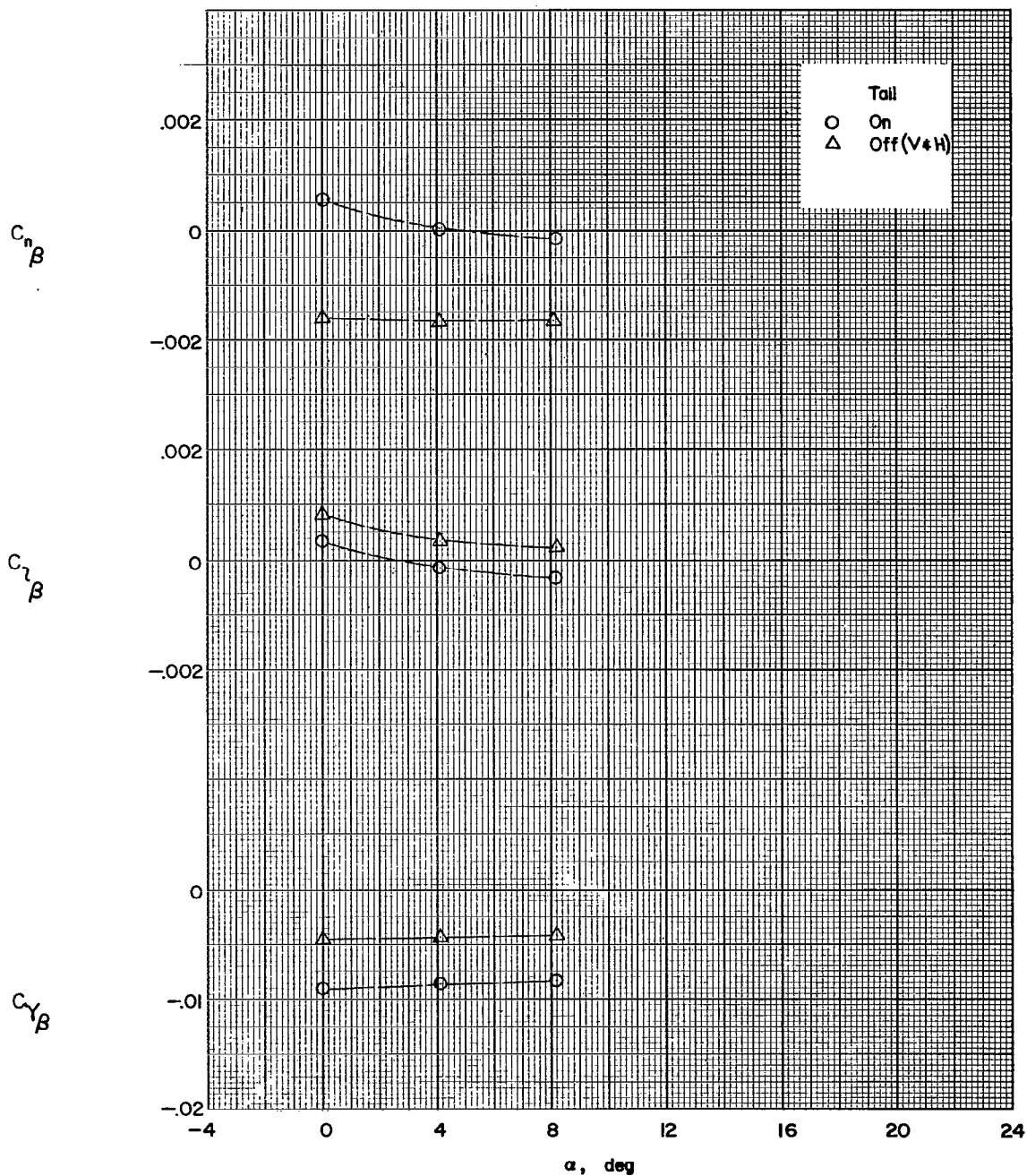


Figure 14.- Variation of sideslip derivatives with angle of attack.  
Basic tail;  $M = 2.01$ .

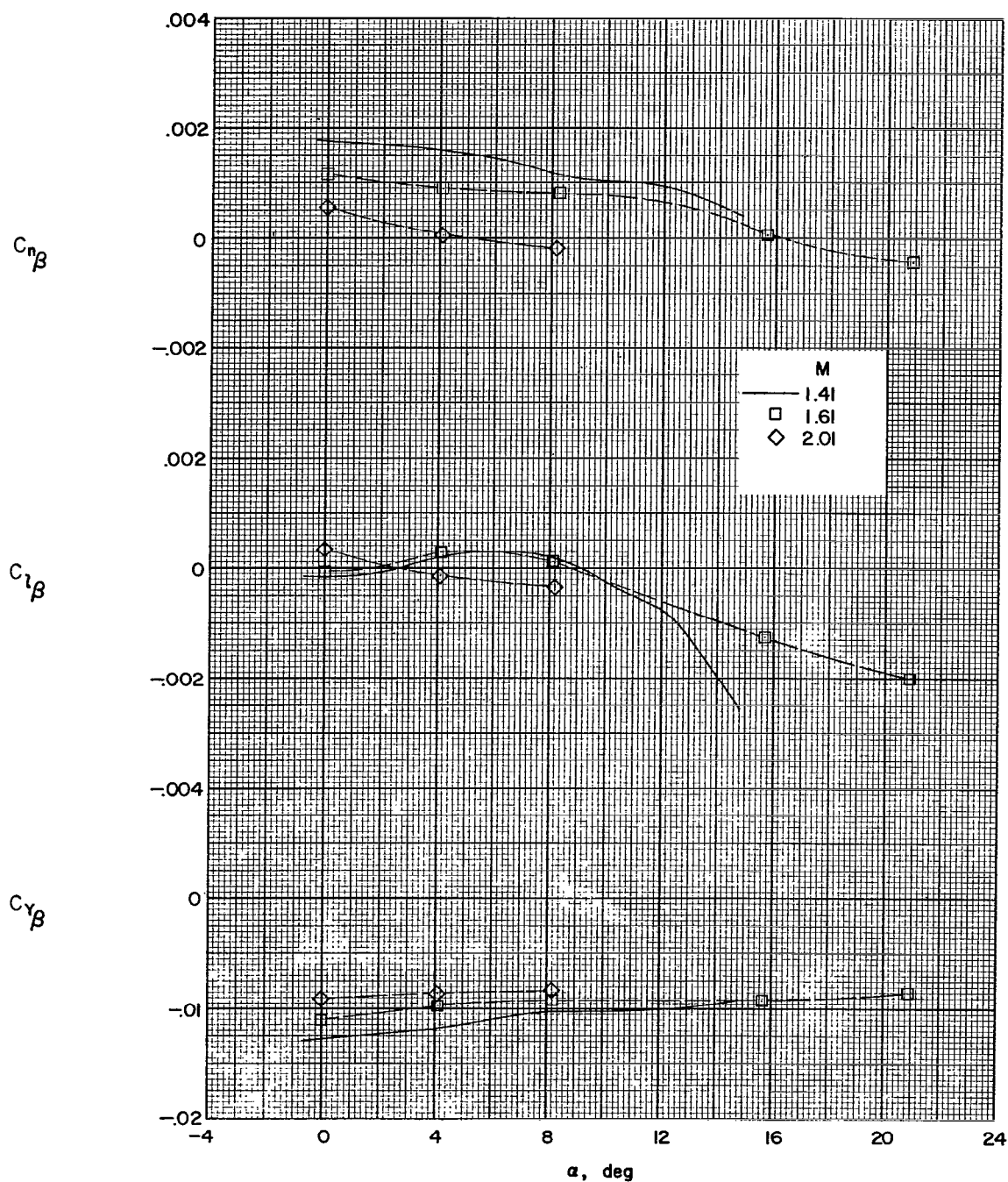


Figure 15.- Variation of sideslip derivatives with angle of attack for various Mach numbers. Basic tail; horizontal tail on.

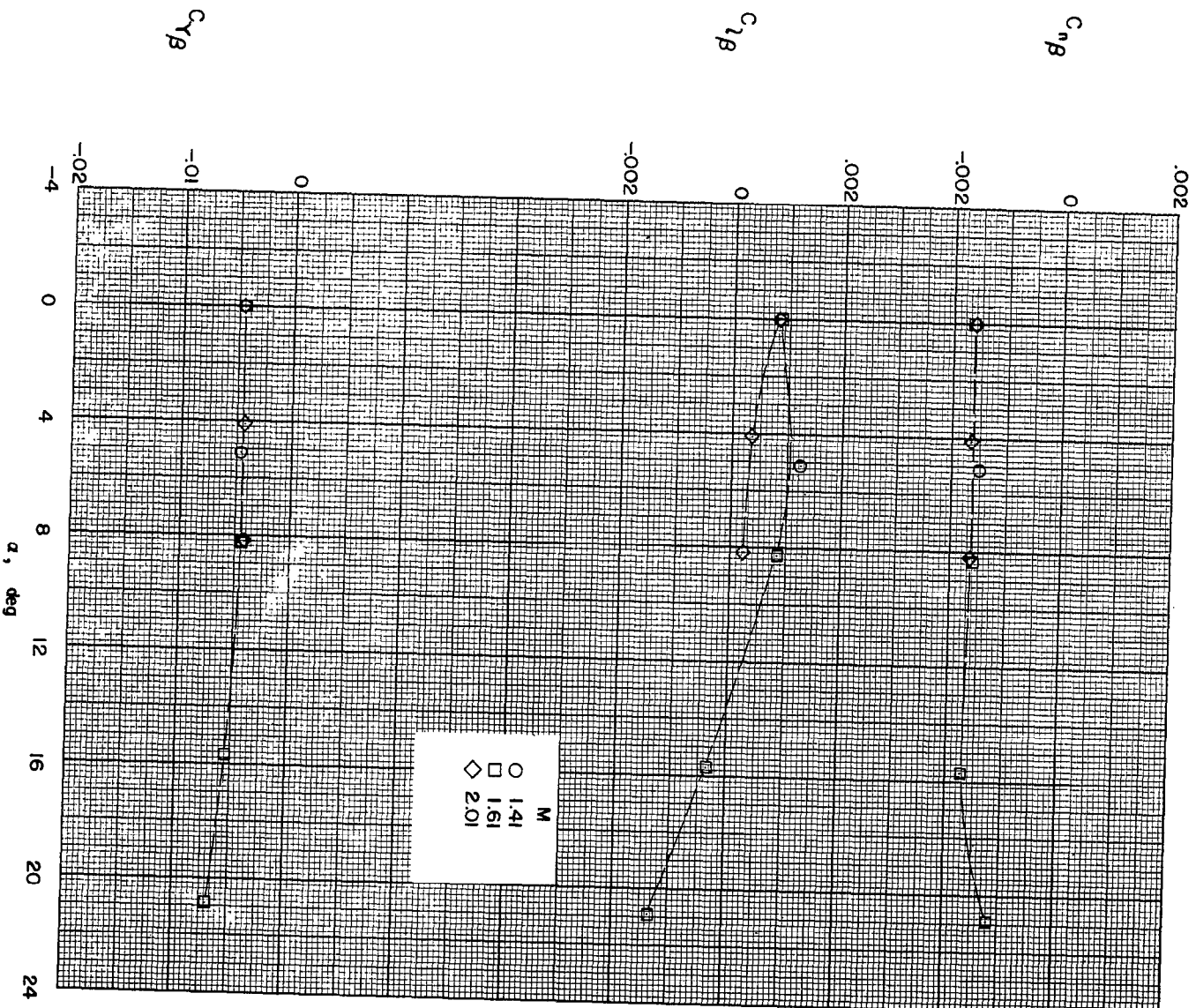


Figure 16.- Variation of sideslip derivatives with angle of attack for various Mach numbers. Vertical and horizontal tails off.

CONFIDENTIAL

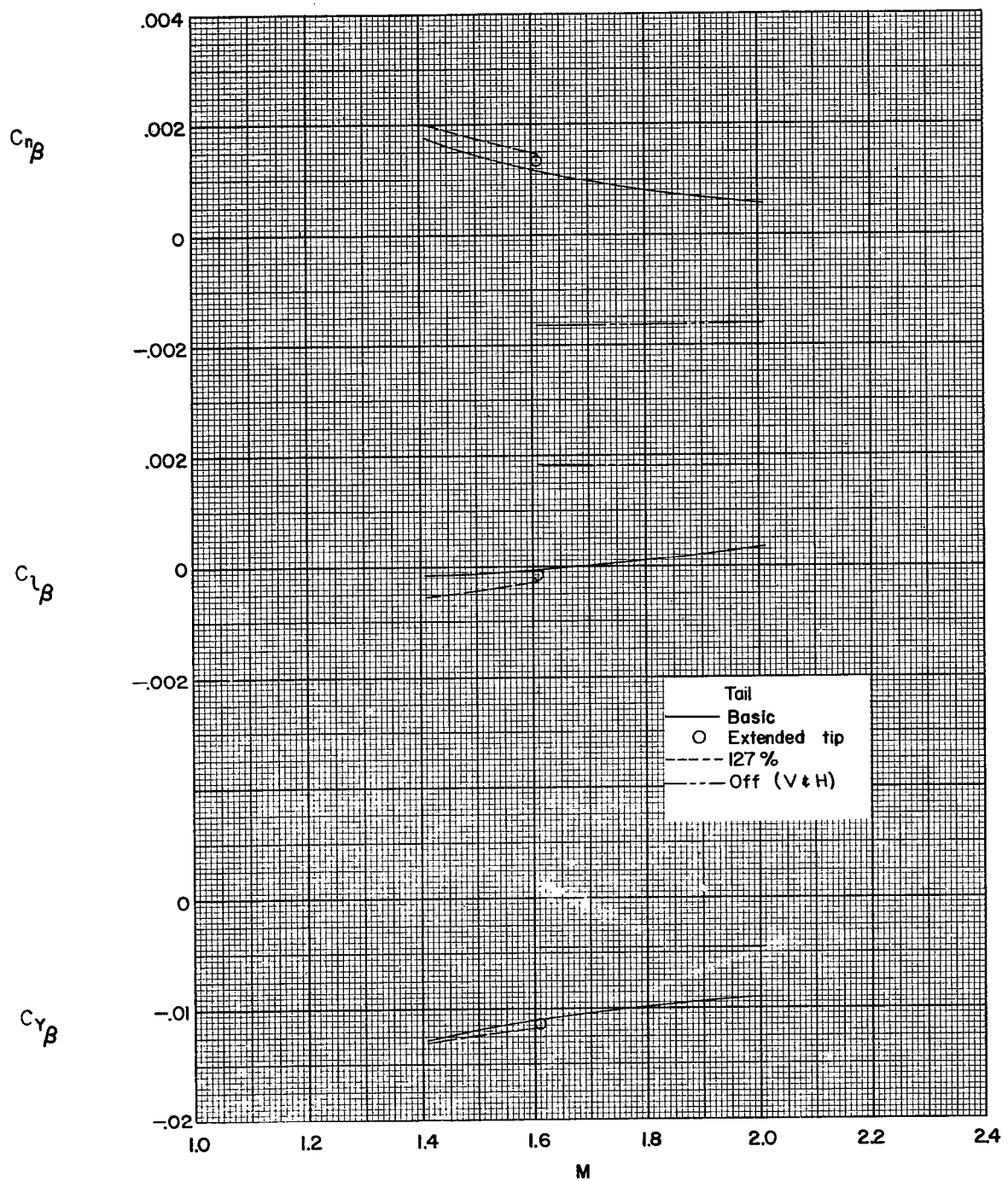


Figure 17.- Variation of sideslip derivatives with Mach number.  $\alpha = 0^\circ$ .

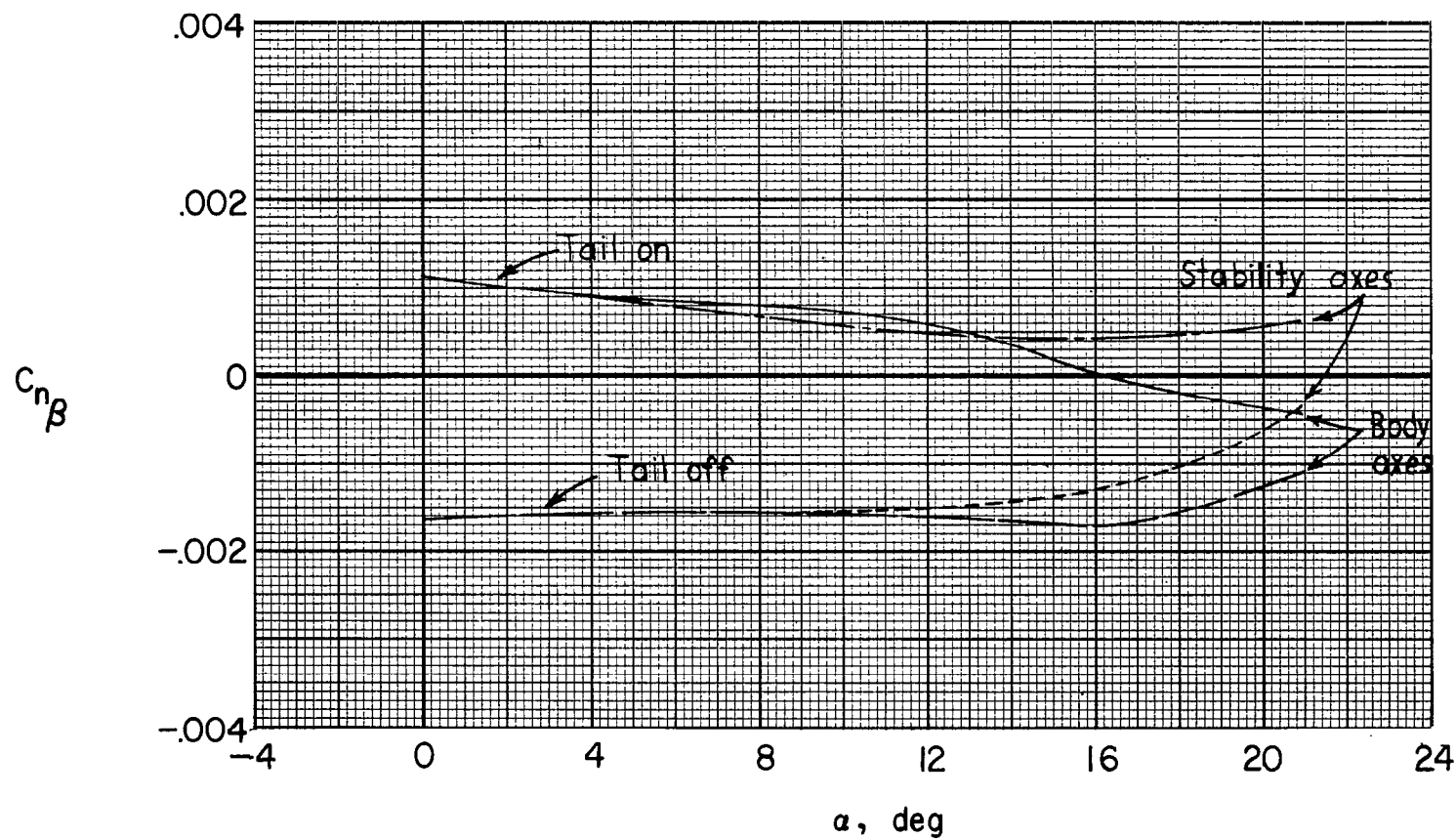
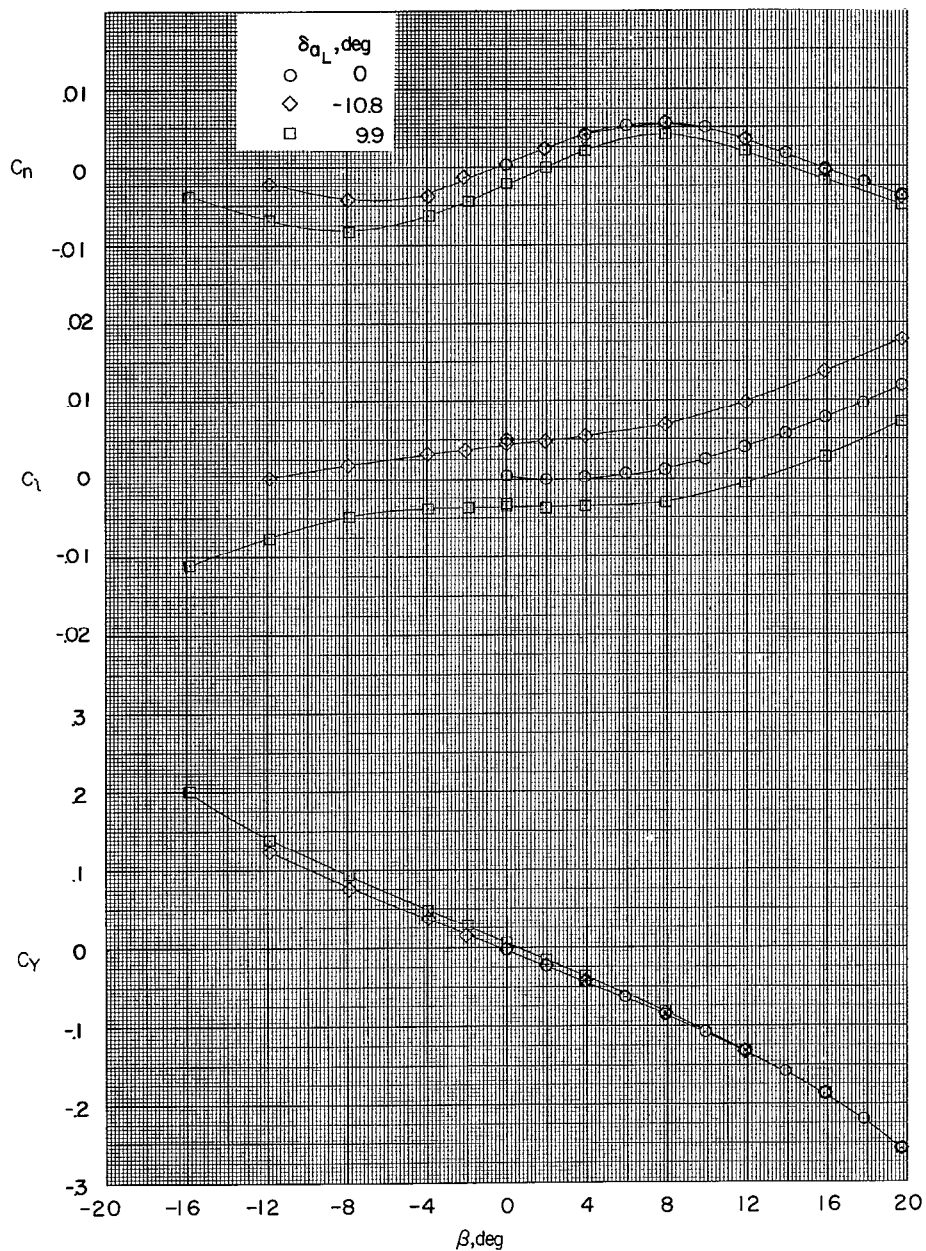


Figure 18.- Effect of axis system on the variation of  $C_{n\beta}$  with angle of attack. Basic tail;  $M = 1.61$ .





(a)  $\alpha = 0^\circ$ .

Figure 19.- Effect of aileron deflection on aerodynamic characteristics in sideslip at various angles of attack. Basic tail;  $M = 1.61$ .



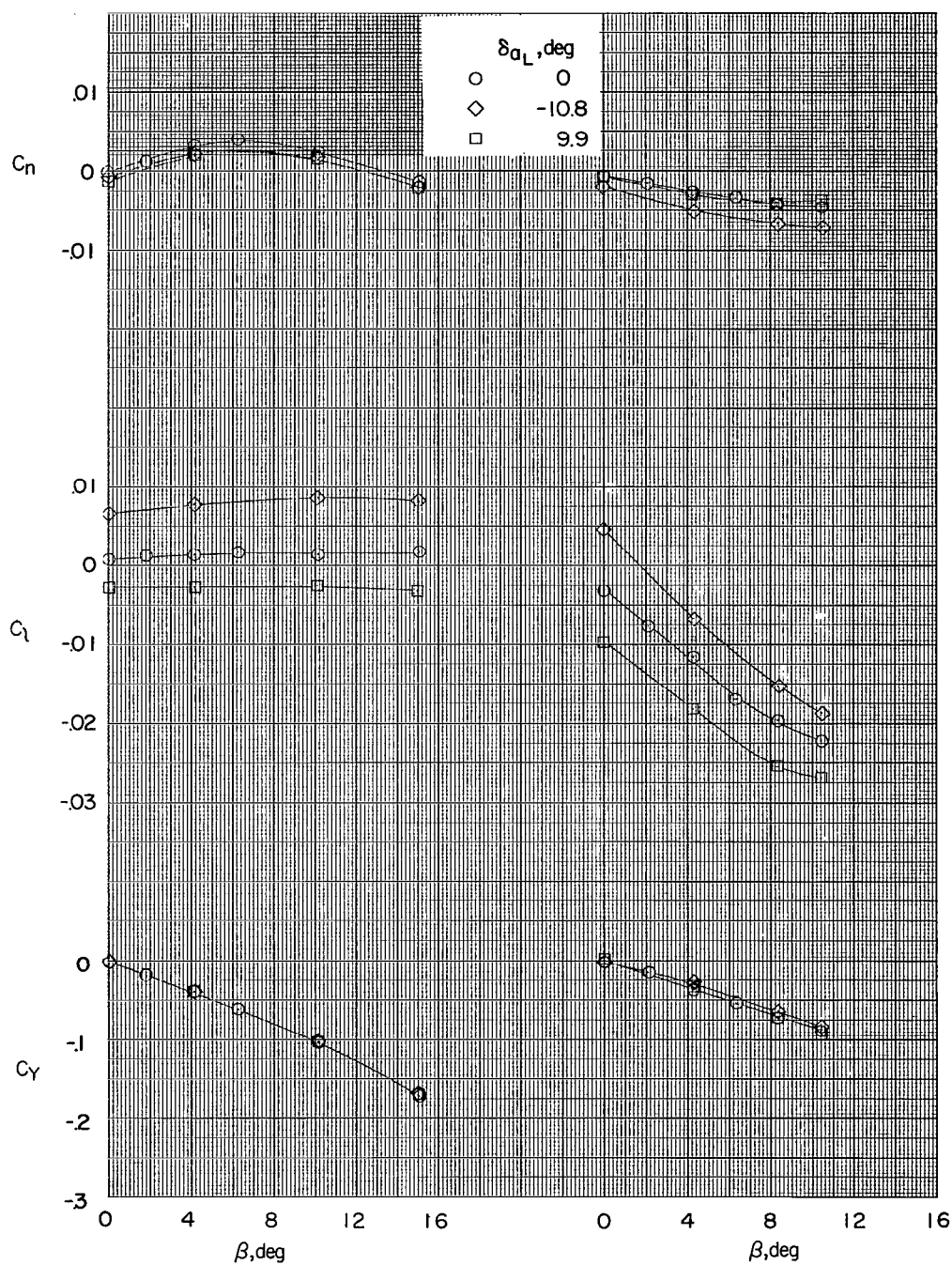
(b)  $\alpha = 8.3^\circ$ .(c)  $\alpha = 20.9^\circ$ .

Figure 19.- Concluded.

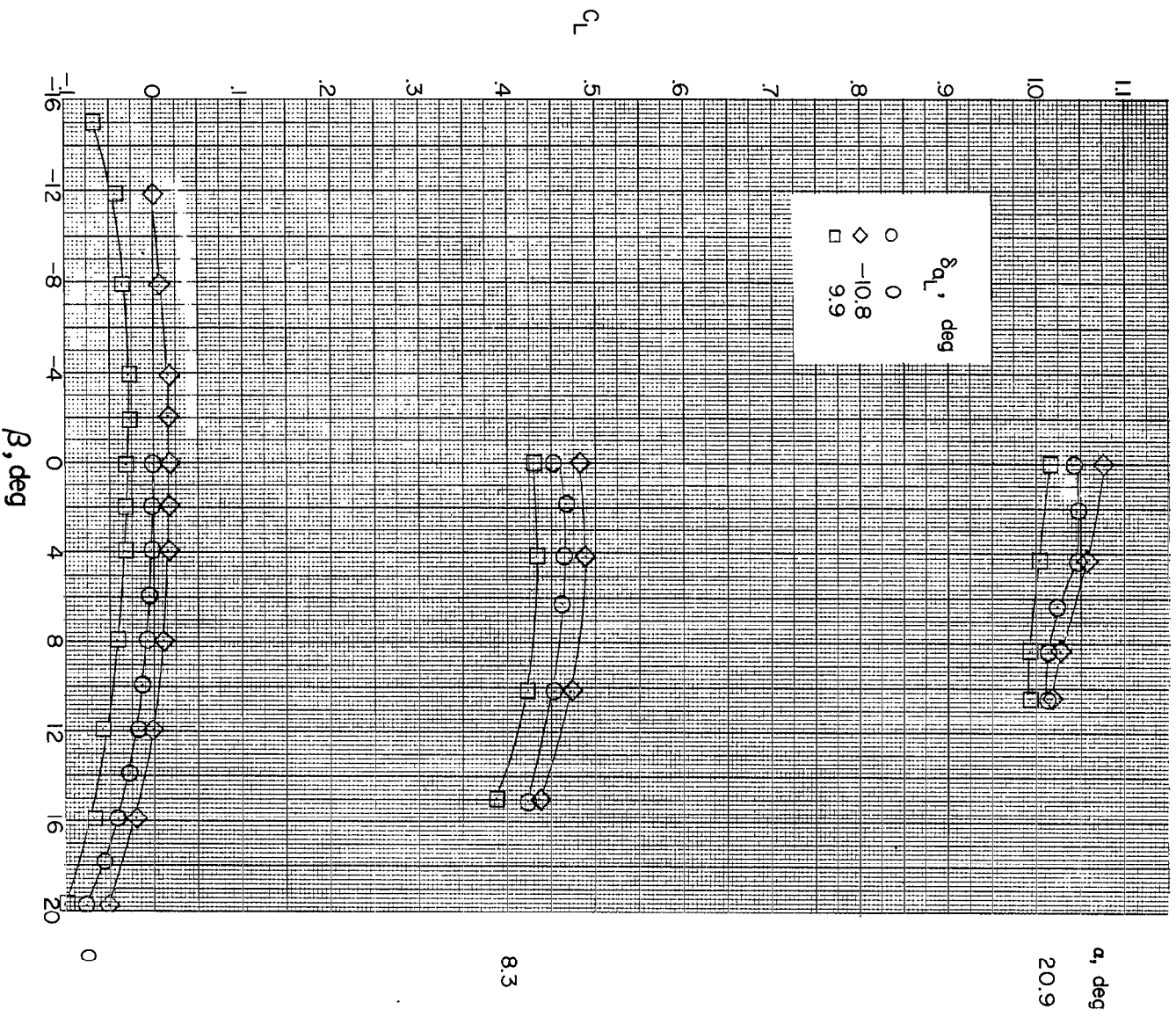


Figure 20.- Effect of aileron deflection on the variation of the lift, longitudinal-force, and pitching-moment coefficients with sideslip for various angles of attack. Production tail;  $i_t = 0^\circ$ ;  $M = 1.61$ .

CONFIDENTIAL

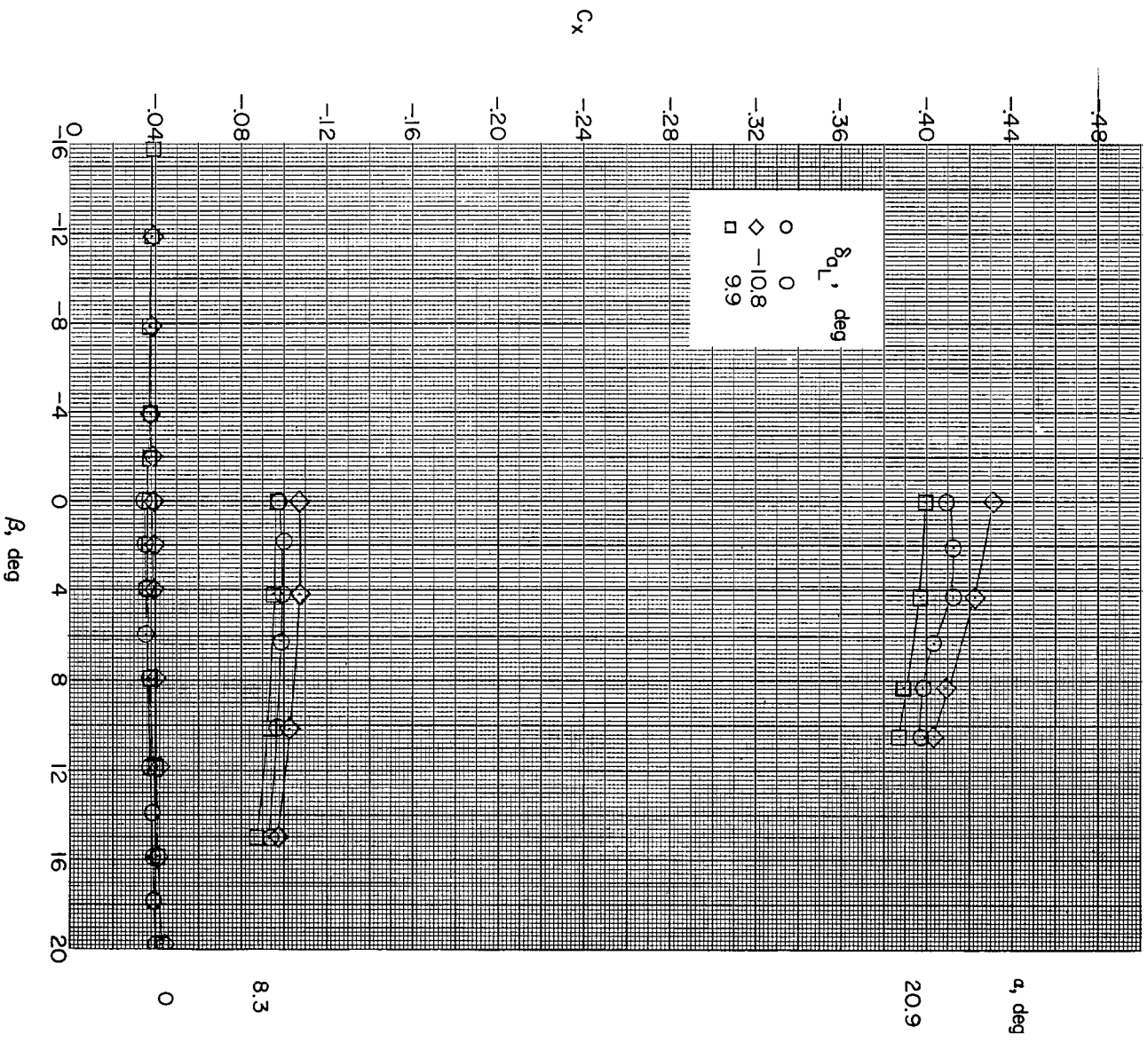


Figure 20.- Continued.

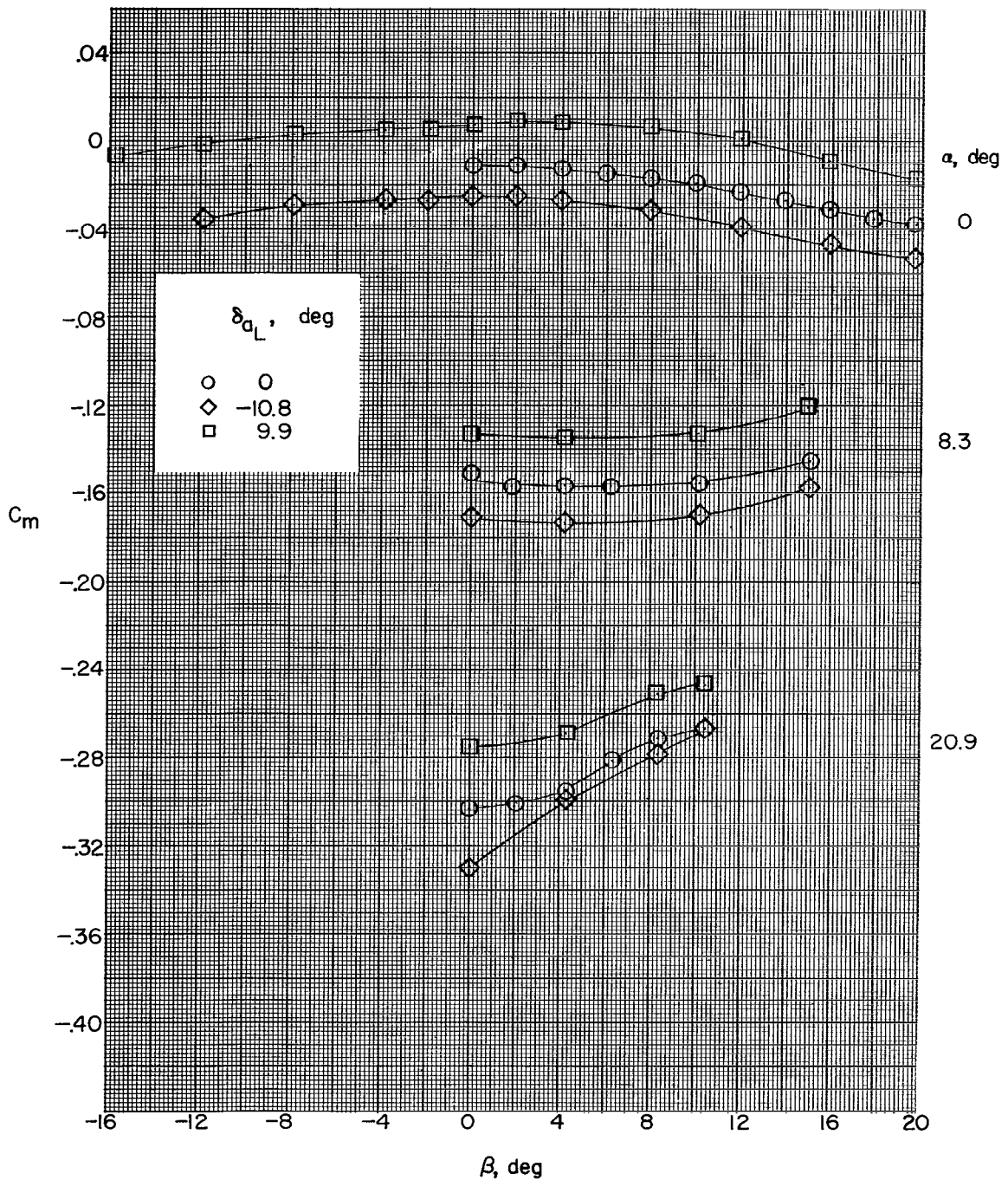


Figure 20.- Concluded.

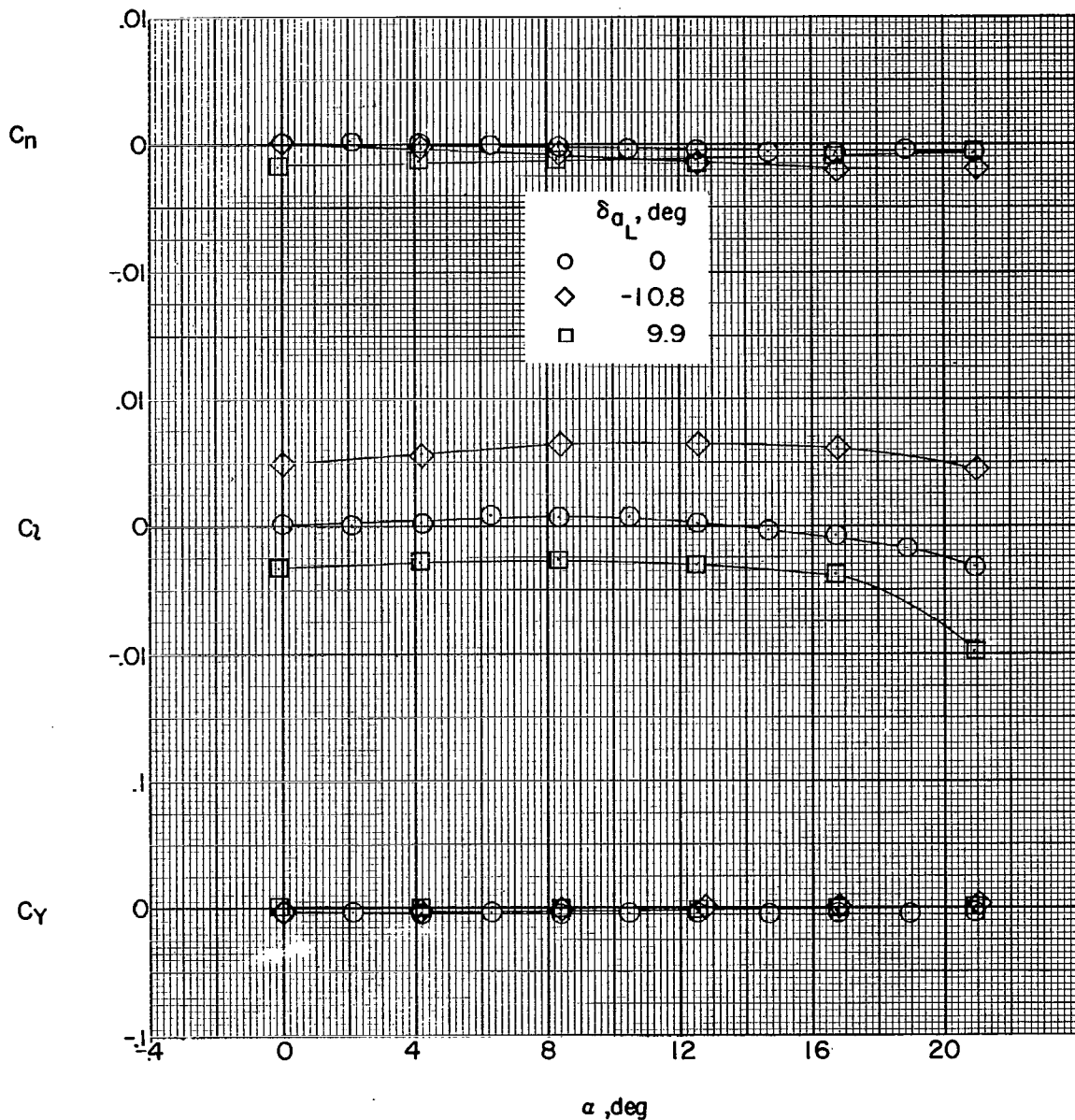


Figure 21.- Effects of angle of attack on aileron-control characteristics.  
Basic tail;  $\beta = 0^\circ$ ;  $M = 1.61$ .

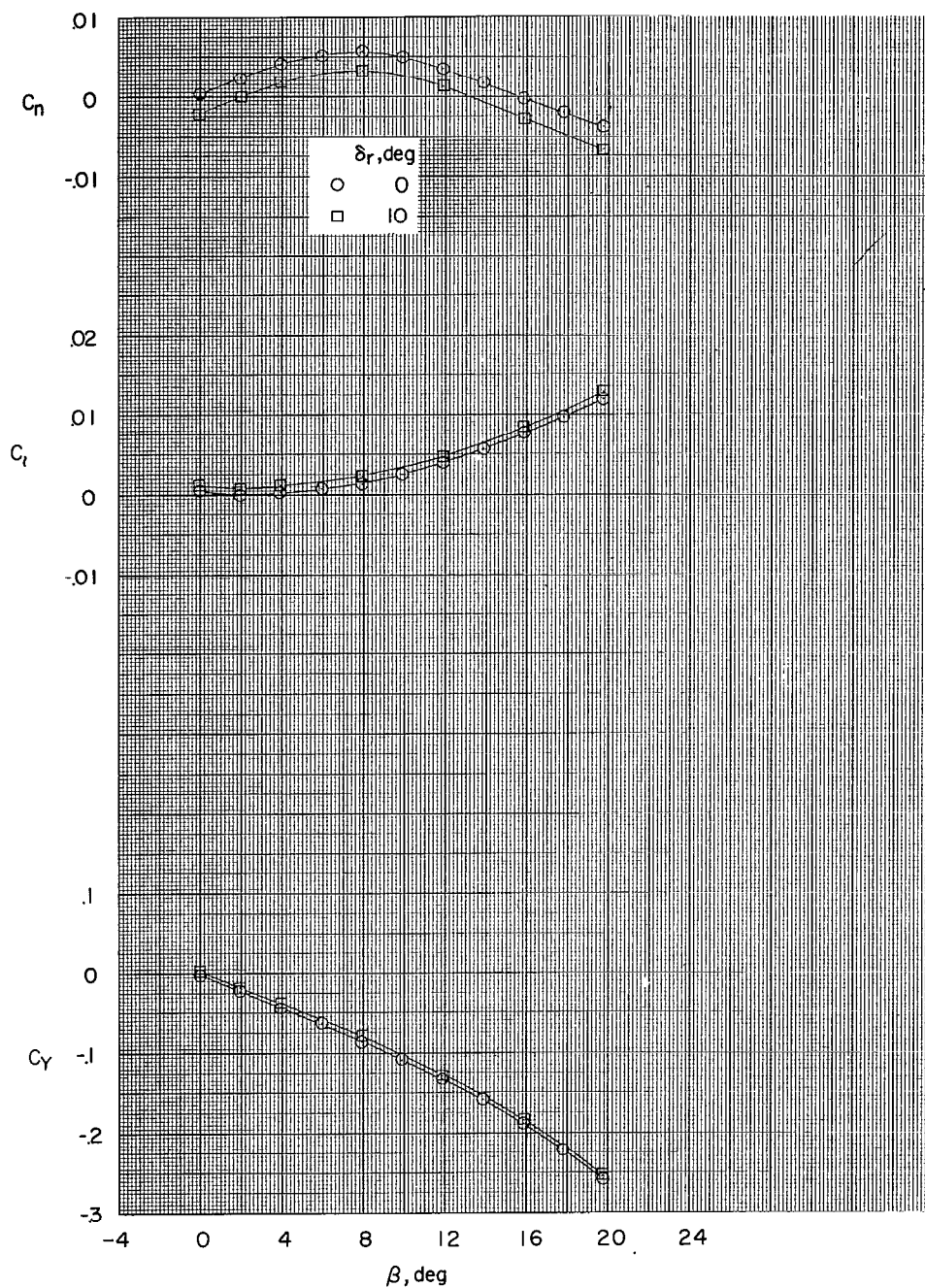
(a)  $\alpha = 0^\circ$ .

Figure 22.- Effects of rudder deflection on aerodynamic characteristics in sideslip at various angles of attack. Basic tail;  $M = 1.61$ .

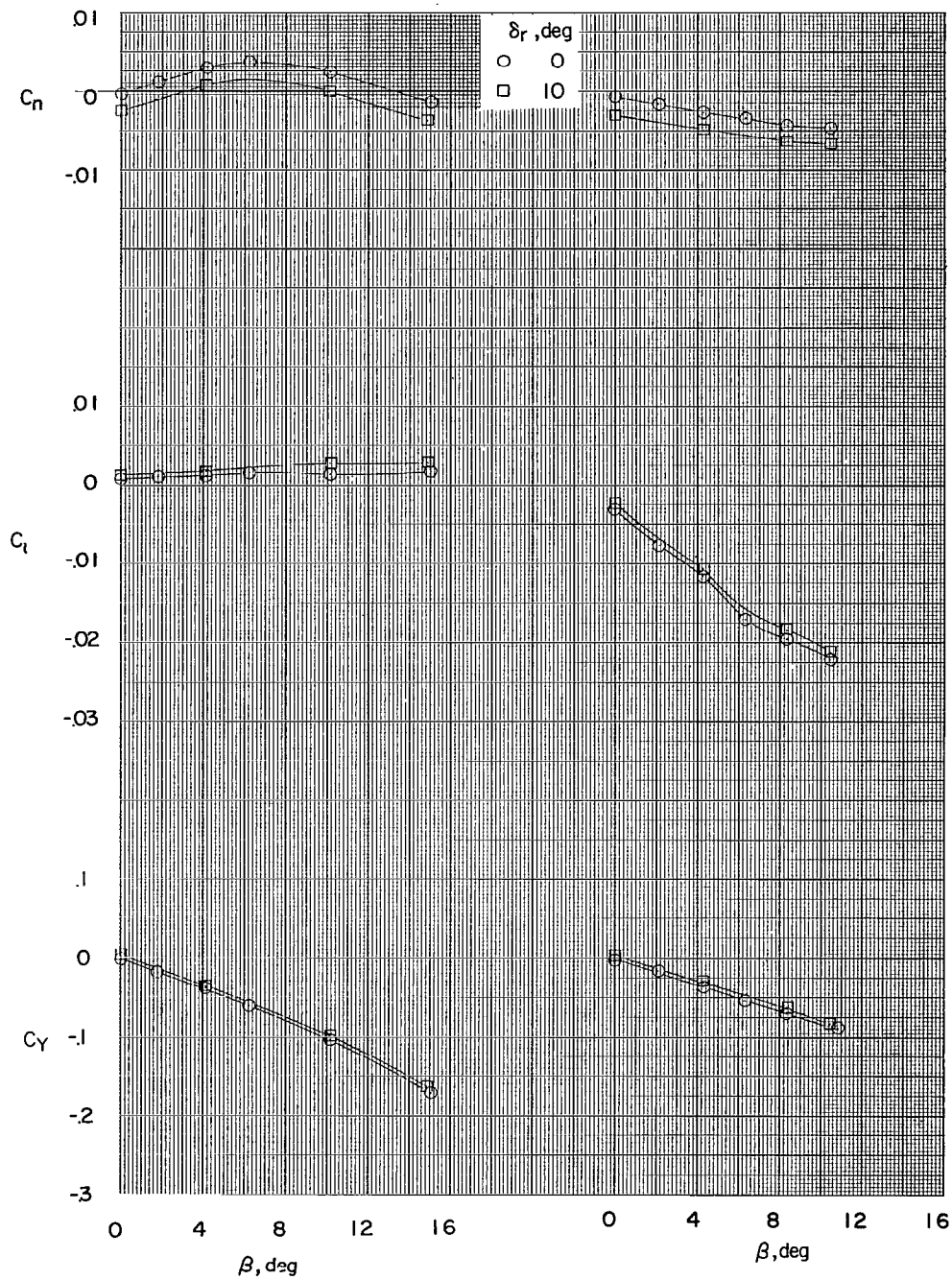
(b)  $\alpha = 8.3^\circ$ .(c)  $\alpha = 20.9^\circ$ .

Figure 22.- Concluded.



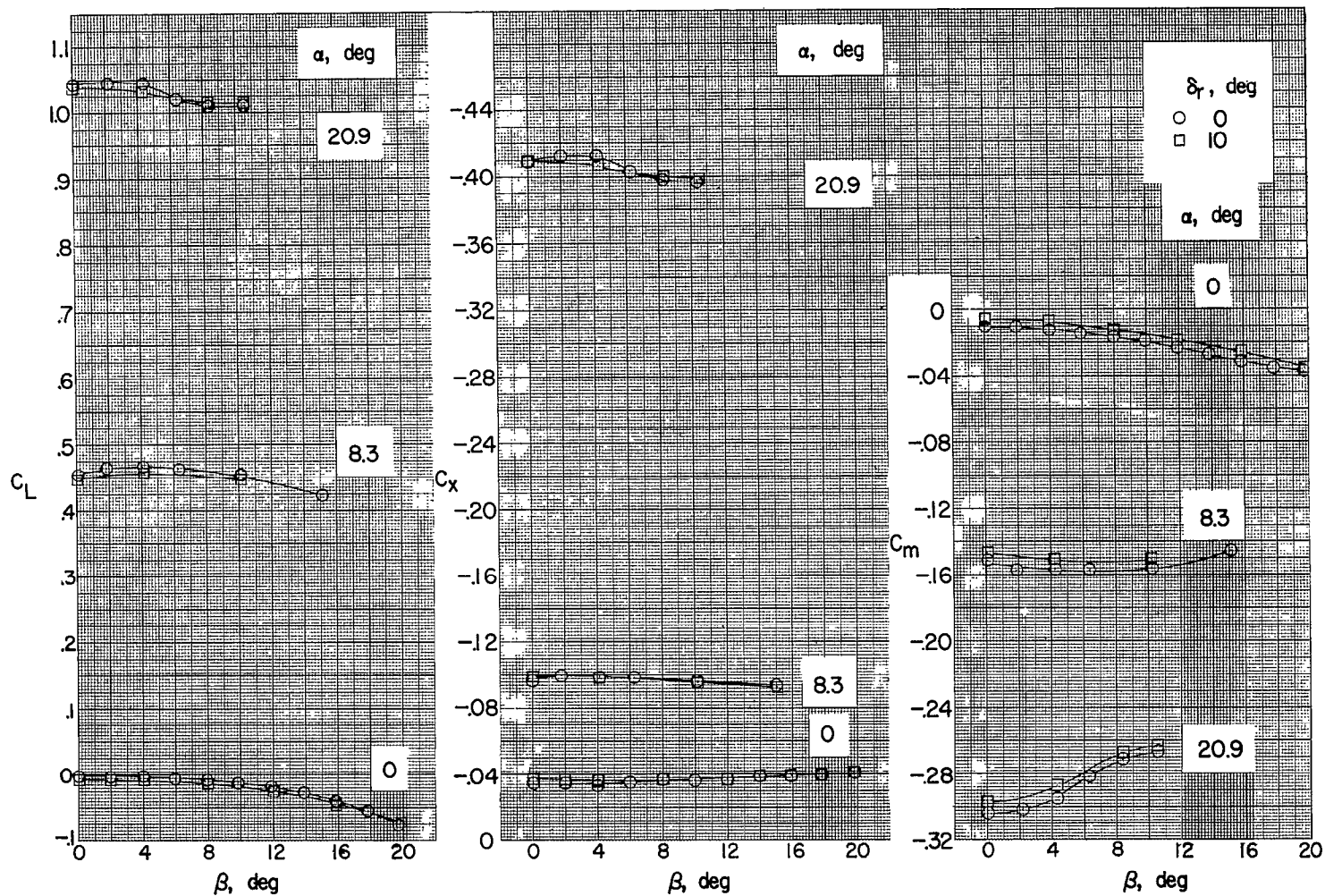


Figure 23.- Effects of rudder deflection on the variation of lift, longitudinal-force, and pitching-moment coefficients in sideslip for various angles of attack. Basic tail;  $i_t = 0^\circ$ ;  $M = 1.61$ .



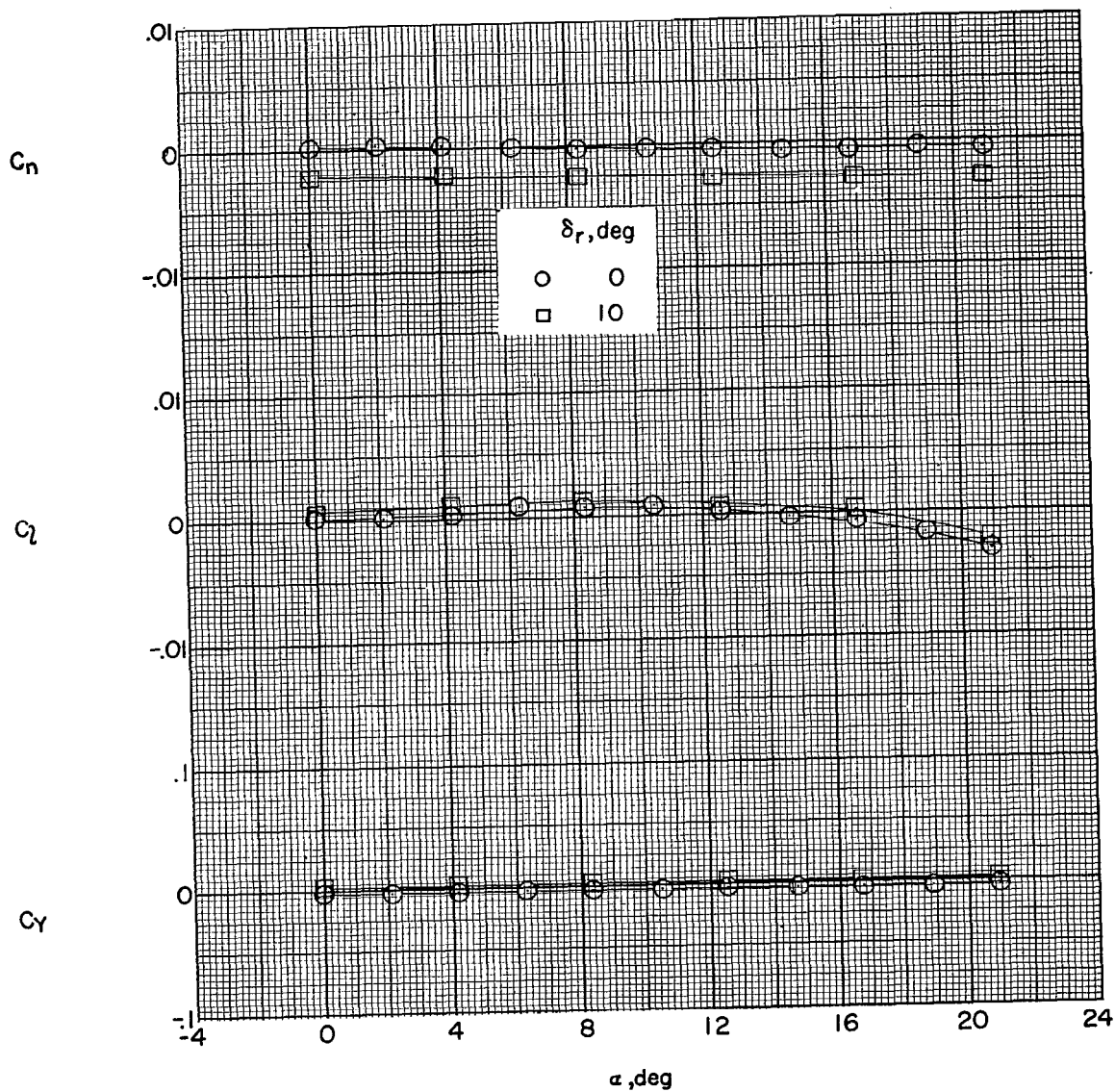


Figure 24.- Effects of angle of attack on rudder-control characteristics.  
Basic tail;  $\beta = 0^\circ$ ;  $M = 1.61$ .

NASA Technical Library



3 1176 01437 2172

~~CONFIDENTIAL~~